Czech Technical University in Prague

Faculty of Civil Engineering

Department of Mechanics

Numerical modeling of fresh concrete flow and description of formwork pressures

Kryštof Kout

Bachelor Thesis

Supervisor: Ing. Jiří Němeček, Ph.D.

Year: Prague, 2024

BACHELOR‘S THESIS ASSIGNMENT

I. Personal and study details

Student's name: **Kout Kryštof** Personal ID number: **501907**

Faculty / Institute: **Faculty of Civil Engineering**

Department / Institute: **Department of Mechanics**

Study program: **Civil Engineering**

Specialisation: **Architectural Engineering**

II. Bachelor’s thesis details

Bachelor’s thesis title in English:

Numerical modeling of fresh concrete flow and description of formwork pressures

Bachelor’s thesis title in Czech:

Numerické modelování toku čerstvého betonu a popis tlaků na bednění

Guidelines:

Learning about CFD modeling, fluid-solid interaction, material models for concrete, its flow and thixotropy, and subsequent implementation to Ansys. Conducting parametric study and evaluation of key parameters affecting formwork pressures and comparison with existing experiments.

Bibliography / sources:

Roussel, N. (2006). A thixotropy model for fresh fluid concretes: Theory, validation and applications. Cement and concrete research, 36(10), 1797-1806.
Larson, R. G., & Wei, Y. (2019). A review of thixotropy and its rheological modeling. Journal of Rheology, 63(3), 477-501.
Roussel, N., Ovarlez, G., Garrault, S., & Brumaud, C. (2012). The origins of thixotropy of fresh cement pastes. Cement and Concrete Research, 42(1), 148-157.

Name and workplace of bachelor’s thesis supervisor:

Ing. Jiří Němeček, Ph.D. Department of Mechanics FCE

Name and workplace of second bachelor’s thesis supervisor or consultant:

Date of bachelor’s thesis assignment: **22.02.2024** Deadline for bachelor thesis submission: **20.05.2024**

Assignment valid until: _____

Ing. Jiří Němeček, Ph.D.	prof. Ing. Jiří Máca, CSc.	prof. Ing. Jiří Máca, CSc.
Supervisor's signature	Head of department's signature	Dean's signature

III. Assignment receipt

The student acknowledges that the bachelor’s thesis is an individual work. The student must produce his thesis without the assistance of others, with the exception of provided consultations. Within the bachelor’s thesis, the author must state the names of consultants and include a list of references.

Date of assignment receipt	Student’s signature

Declaration

I hereby declare that this bachelor thesis has been my own work, written under supervision of Ing. Jiří Němeček, Ph.D.

All sources of information that have been used in the bachelor thesis are acknowledged in the text and listed in the Bibliography.

In Prague, May 2024

.....

Kryštof Kout

Acknowledgements

I would like to express my sincere gratitude to all those who supported me throughout the completion of this bachelor thesis.

First and foremost, I am deeply thankful to my supervisor, Ing. Jiří Němeček, Ph.D., for giving me an idea of the topic of this thesis, for his invaluable guidance, encouragement, and excellent feedback during frequent consultations.

I am also very grateful to Ing. Pavel Trávníček, Ph.D., for his assistance in learning the basics of programming and creating the numerical model and prof. Ing. Jiří Němeček, Ph.D., DSc., for provision of experimental data and lending a powerful computer for complex calculations.

Finally, I wish to acknowledge the support of my family and friends for their encouragement and understanding during this academic journey.

The work was inspired and financially supported by the project of the Technology Agency of the Czech Republic Trend No. FW01010521, solved as a cooperation project of Czech Technical University in Prague, Skanska a.s., and Skanska Transbeton s.r.o. company.

Abstract

In this thesis, the main objective was to create a model of a wall that describes the flow of self-compacting concrete and calculates the resulting pressure on the formwork. Several submodels were developed to test individual components of the final concrete flow model. First, a cantilever was modeled to calculate deflection and normal stress in Ansys Mechanical. Next, the fluid flow experiment of water filling a tank was modeled using Ansys Fluent and the volume of fluid model. Subsequently, the slump flow test was modeled using the Herschel-Bulkley model for different cement pastes. Three wall models were created to determine the suitable wall geometry and filling method. Then, a 2D model of the longitudinal wall section was created to assess how the concrete flows around the problematic corner of the window. Lastly, a one-way fluid-structure interaction (FSI) model of the wall was made. The results indicate that the Herschel-Bulkley model reliably replicates the slump flow experiments. However, it proves inadequate for accurately estimating pressure on the formwork, as it significantly overestimates calculated pressures compared to the experiment. Further correction is necessary by incorporating a material model that considers thixotropy and material aging. Mixtures with high yield stress thresholds lead to poor concrete surface quality. The presented one-way FSI calculates equivalent (von-Mises) stress and deformation of the formwork. However, these values appear almost independent of the concrete mixture.

Keywords

Concrete, concrete wall, self-compacting concrete, thixotropy, fluid-structure interaction, computational fluid dynamics, volume of fluid.

Abstrakt

Hlavním cílem této práce bylo vytvořit model stěny, který popisuje tok samozhutnitelného betonu a vypočítává výsledný tlak na bednění. Bylo vytvořeno několik dílčích modelů pro testování jednotlivých složek finálního modelu toku betonu. Nejprve byla modelována konzola pro výpočet průhybu a normálového napětí v programu Ansys Mechanical. Dále byl modelován experiment proudění kapaliny plnící nádrž pomocí programu Ansys Fluent a modelu objemu kapaliny. Následně byla vymodelována zkouška sednutí kužele pomocí Herschel-Bulkleyho modelu pro různé cementové pasty. Byly vytvořeny tři modely stěn pro určení vhodné geometrie stěn a způsobu plnění. Poté byl vytvořen 2D model podélného řezu stěny, aby bylo možné posoudit, jak beton protéká kolem problematického rohu okna. Nakonec byl vytvořen jednosměrný model interakce tekutiny s konstrukcí (FSI) stěny. Výsledky ukazují, že Herschel-Bulkleyho model spolehlivě replikuje experimenty se sednutím betonu. Ukázalo se však, že pro přesný odhad tlaku na bednění je nedostatečný, protože ve srovnání s experimentem výrazně nadhodnocuje vypočtené tlaky. Další korekce je nutná začleněním materiálového modelu, který zohledňuje tixotropii a stárnutí materiálu. Směsi s vysokými mezemi kluzu vedou ke špatné kvalitě povrchu betonu. Předložená jednosměrná FSI počítá ekvivalentní (von-Misesovo) napětí a deformaci bednění. Tyto hodnoty se však jeví jako téměř nezávislé na betonové směsi.

Klíčová slova

Beton, betonová stěna, samozhutnitelný beton, tixotropie, interakce kapaliny s konstrukcí, výpočetní dynamika tekutin, objem kapaliny.

List of Figures

List of Tables

Abbreviations

AC	**A**nsys **C**alculation
AS	**A**nalytical **S**olution
CFD	**C**omputational **F**luid **D**ynamics
FEM	**F**inite **E**lement **M**ethod
FSI	**F**luid-**S**tructure **I**nteraction
MK	**M**eta**K**aolin
SCC	**S**elf-**C**ompacting **C**oncrete
VOF	**V**olume **O**f **F**luid

Symbols

F	Force	(N)
τ	Shear stress	(Pa)
$\dot{\gamma}$	Shear rate	(s^{-1})
μ	Viscosity	($m^2 \cdot s^{-1}$)
τ_0	Yield stress threshold	(Pa)
μ_∞	Coefficient of rigidity	($m^2 \cdot s^{-1}$)
μ_p	Plastic viscosity	(Pa·s)
$\dot{\gamma_0}$	Critical shear rate	(s^{-1})
k	Consistency index	($Pa \cdot s^n$)
n	Power-law coefficient	(-)
λ	Flocculation state	(-)
v	Velocity	($m \cdot s^{-1}$)
t	Time	(s)
p	Static pressure	(Pa)
ρ	Density	($kg \cdot m^{-3}$)
g	Gravitational acceleration	($m \cdot s^{-2}$)
w	Deflection	(m)
L	Length	(m)
W	Width	(m)
T	Thickness	(m)
E	Young´s modulus	(Pa)
I	Moment of inertia	(m^4)
w/c	Water/cement ratio	(-)

Contents

1 Introduction

The main objective of this thesis is to address issues related to tall concrete walls. These walls are typically over 6 meters in height and are made of self-compacting concrete (SCC) [1–3] which requires a high surface quality. An example of a wall made from SCC can be seen in Figure 1.1. The primary issue is that these concrete mixtures exert high lateral pressure on the formwork at the bottom of the wall, causing damage to both the formwork and the wall itself. There are two main approaches to solving this problem.

Figure 1.1: Example of a real-life faced concrete wall made out of self-compacting concrete on-site.

The first approach requires adjusting and strengthening the formwork. The typical formwork for a standard tall wall can be seen in Figure 1.2. However, further strengthening of the formwork is too expensive and unnecessarily complicated to assemble.

The second approach involves further adjustment of the concrete mix. The mix needs to be liquid enough to flow into the formwork easily and meet the required visual surface

Figure 1.2: Example of a formwork of wall made out of self-compacting concrete on-site.

quality, but for the lateral pressure to be low, the mix needs to be sufficiently rigid. Therefore, more than an adjustment of the water/cement ratio or adding admixtures is required. This contradiction can be resolved by designing the concrete mix to be thixotropic. Thixotropic concrete means that the mix is liquid when it is poured out of the concrete bucket, but as soon as it stops moving in the formwork, it becomes rapidly more rigid [4, 5]. Acquiring this property in the concrete mix is the most appropriate solution, as it meets all the concrete's requirements and addresses all the formwork's problems. This material property can be achieved by using special additives such as metakaolin (MK), sepiolite, or nanoclays [6–8].

1.1 Thesis motivation

Testing a large number of mixtures is not an easy task in real-life experiments because their behavior differs significantly depending on the size of the experiment. More precisely, the thixotropic behavior cannot be reasonably compared between laboratory testing and on-site conditions. Unfortunately, testing a large number of mixtures only on-site is too expensive.

For this reason, a numerical model of a full-size wall has been developed in this thesis. The main purpose of the model is to test a large number of SCC mixtures with different thixotropic additives to calculate the lateral pressure on the formwork, and formwork deformation, and estimate the resulting visual surface quality of the finished concrete.

1.2 Research objectives

The main purpose of this thesis was to create a numerical model of a full-sized wall that accurately describes the fresh concrete flow into the formwork and calculates the resulting pressure on the formwork using the volume of fluid (VOF) model and fluid-structure interaction (FSI). The task was initially divided into a series of sub-tasks to learn how to correctly use Ansys software and perform numerical modeling. The main objectives of the thesis are as follows:

- To create a static structural Finite Element Method model of a concrete wall, calculate deformation, and verify the model with an analytical solution.
- To gain proficiency in using the VOF model and create a simulation task involving the exchange between two fluid phases, such as water and air.
- To conduct a slump flow test on a cement paste using a non-Newtonian fluid material model, and compare the results to the experimental data.
- To create a model of a full-sized wall that describes SCC flow, enables the assessment of the visual surface quality of the faced concrete and estimates the pressure within the mixture.
- To create a one-way FSI model of a full-sized wall that describes the SCC flow, calculates the lateral pressure on the formwork and estimates the deformation and stress of the formwork.

2 Theory

2.1 Fresh concrete mix

Self-compacting concrete (SCC), also known as self-consolidating concrete in North America, is a specialized type of concrete designed for ease of use in its fresh state. SCC has the unique ability to flow into a formwork under its weight without needing external force and vibration, and without segregating, making it highly convenient for construction. Important characteristics of fresh SCC include its ability to effortlessly fill complex formwork, which is useful, especially in cases of difficult geometry or highly reinforced objects. SCC is essentially a mixture of particles suspended within a fluid matrix. The composition of SCC can vary significantly between countries due to local and available resources, impacting final concrete properties like strength, shrinkage, and durability. Challenges and opportunities associated with SCC include ensuring sustainability, durability, and compatibility of materials as well as developing effective flow modeling and mix design techniques [1–3].

2.2 Types of tests for testing the consistency of fresh concrete mix

Consistency testing is crucial in assessing the workability and flow properties of concrete and SCC mixes. Various tests, such as the Slump flow test, L-Box test, U-Box test, or J-Ring test are employed to evaluate these rheological properties and ensure optimal performance in different applications.

2.2.1 Slump flow test

The slump flow test is a standard method used to measure the consistency and workability of fresh concrete. It involves filling a mold with freshly mixed concrete and then removing the mold to observe the slump or subsidence of the concrete. The results of this test can be seen in Figure 2.1.

a) b)

Figure 2.1: Results of slump flow test using different cones a) Abrams, b) Hagermann.

Using an Abrams cone in this test is suitable for traditional concrete mixes and provides insights into their flow characteristics. The slump flow test categorizes concrete consistency

into five classes S1–S5, ranging from very low to very high. Class S1, with a slump of 10–40 mm, indicates the lowest consistency and is used for applications like road pavements and foundations. At the highest end, with a slump greater than 220 mm, Class S5 represents a very high consistency suitable for self-compacting concrete and areas with difficult access [9].

For the SCC mixtures, the test uses a modified Abrams cone in most cases. Hagermann cone is another often used type of cone [10, 11]. For SCC, the categorization of flowability is divided into three classes: SF1, with a slump flow of 550–650 mm; SF2, with a slump flow of 660–750 mm; and SF3, with a slump flow of 760–850 mm. Mixtures in these classes are suitable for use in complex formworks and heavily reinforced structures [9, 12]. Every tool needed for the execution of the slump flow test using the Hagermann mini-cone can be seen in Figure 2.2.

a) b)

Figure 2.2: a) Hagermann flow table, b) Hagermann flow table with its equipment, notably the mini-cone.

2.2.2 L-Box test

This test assesses the flow of SCC through reinforcing bars, simulating the conditions encountered in structural elements. The L-box apparatus consists of a vertical and horizontal section forming a letter L shape. Concrete is allowed to flow from the vertical section through bars into the horizontal section. The height of the concrete at the end of the horizontal section compared to the height remaining in the vertical section indicates the concrete's ability to pass through reinforcement [12, 13].

2.2.3 U-Box test

This test evaluates the filling ability of SCC. The U-box apparatus is divided into two sections by a vertical partition with reinforcing bars. Concrete is poured into one section and allowed to flow into the other. The difference in height of the concrete between the two sections indicates its filling ability [12, 13].

2.2.4 J-Ring test

This test measures the passing ability of SCC. A J-ring, fitted with vertical bars, is placed around the Abrams cone used in the slump test. After lifting the cone, the concrete flows through the bars of the J-ring. The difference in height between the concrete inside and outside the ring indicates the concrete's passing ability through obstacles [14].

2.2.5 Column test

This test evaluates the stability and segregation resistance of SCC. A column is filled with concrete, and the column is divided into segments after a set period. The concrete in each segment is weighed to assess the uniformity and potential segregation of the mix [15].

2.2.6 V-Funnel test

This test measures the flow time of SCC through a narrow opening, indicating the concrete's viscosity and flow rate. Concrete is poured into a V-shaped funnel, and the time taken for the concrete to flow through the funnel is recorded. Shorter flow times indicate lower viscosity and better flowability [12, 16].

2.2.7 Flow table test

The Flow table test assesses the flow and consistency of concrete by measuring its ability to spread under its weight. The concrete sample is placed on a flat, circular table and subjected to a specified number of drops. The diameter of the spread is measured to determine flowability. This test is useful for both conventional concrete and SCC, offering insights into their flow and workability [17].

2.2.8 Vebe test

The Vebe test evaluates the workability and consistency of concrete by measuring the time taken for the concrete to consolidate under vibration. This test is particularly suitable for concrete mixes with varying workability requirements and helps optimize the mix design for specific applications [18].

2.2.9 Rheometer

A rheometer is a sophisticated scientific instrument used to measure the rheological properties of materials, particularly fluids and soft solids such as polymers, gels, and pastes. It typically consists of a base with a motor, which holds the sample and applies controlled deformation to the material. The measuring system employs various geometric shapes depending on the type of measurement and the material being tested. Common geometries include concentric cylinders, parallel plates, disks, or cone and plate configurations. They serve to apply deformation and measure the response. A sample holder securely holds the material for testing, often maintaining a specific temperature for stable testing conditions. Sensors

and measurement systems capture the material's response to applied stress or deformation. Precise actuators and motors apply controlled stress or deformation to the material. Data processing software records and analyzes the material's response, enabling the calculation of rheological properties. Rheometer working station can be seen in Figure 2.3. The rheometer is the device in the middle, the rest is computer technology for data collection. Rheometers are designed to provide comprehensive information on viscosity, elasticity, and other rheological properties essential for understanding material behavior and application in various industries [19, 20].

Figure 2.3: Rheometer working station.

The equations used for evaluating rheometer measurements depend on the type of rheometer and the specific rheological properties being analyzed. Common parameters solved are viscosity, shear rate, shear stress, and flow behavior index [19, 20].

2.3 Fluid types

Newtonian fluids exhibit a linear relationship between shear stress and shear rate, with constant viscosity regardless of the applied shear rate. Examples of Newtonian fluids include water and air.

Non-Newtonian fluids, on the other hand, do not follow a linear relationship between shear stress and shear rate. The viscosity of non-Newtonian fluids can change with the applied shear rate or stress. There are various types of non-Newtonian fluids, such as shear-thinning (viscosity decreases with increasing shear rate), shear-thickening (viscosity increases with increasing shear rate), and viscoelastic fluids (exhibiting properties of both liquids and solids). Flow curves of the most common types of fluids can be seen in Figure 2.4.

Concrete is an example of a non-Newtonian fluid. It is a complex fluid with time-dependent and rheological properties, demonstrating non-Newtonian behavior due to its sensitivity to applied stress and strain rates [23].

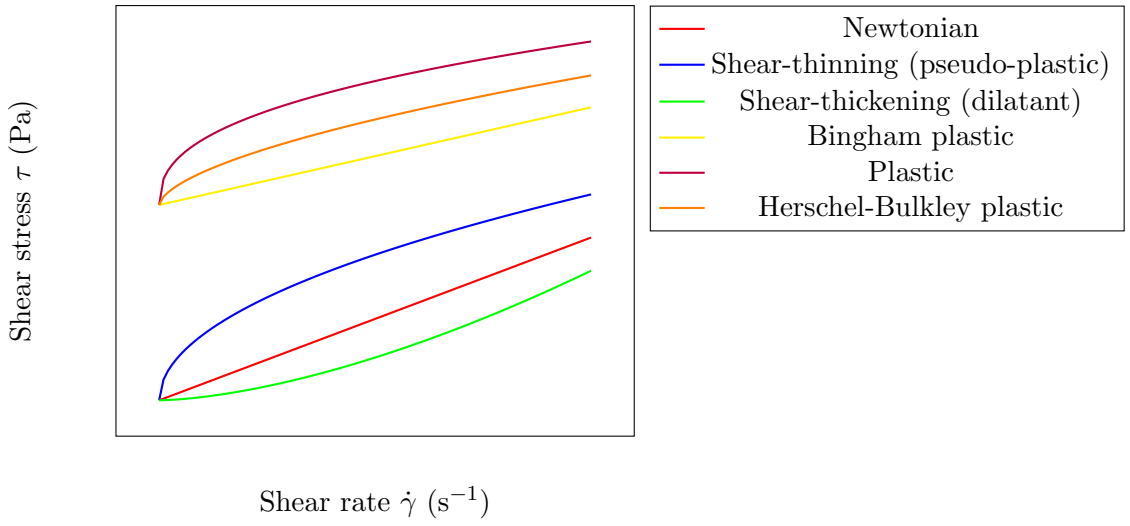

Figure 2.4: Graph showing flow curves of different types of fluids [21, 22].

2.4 Material models

Materials models are important tools that enable simulation of the behavior of concrete mixtures [24].

2.4.1 Bingham plastic model

The Bingham plastic model is the most used material model for the simulation of concrete mixtures. This model is particularly suited for describing the behavior of materials that exhibit yield stress. The flow curve describing the behavior of this model can be seen in Figure 2.4. In the Bingham plastic model, the material begins to flow only when the applied stress exceeds a certain threshold called the yield stress. Once the yield stress is surpassed, the material behaves like a viscous fluid with a linear relationship between stress and strain rate [25]. Its corresponding equation is written as

$$\mu = \tau_0 \left|\dot{\gamma}\right|^{-1} + \mu_\infty, \tag{2.1}$$

where μ is the viscosity, τ_0 is the yield stress threshold, $\dot{\gamma}$ is the shear rate, and μ_∞ is the coefficient of rigidity.

The Bingham plastic model also describes the shear stress as

$$\tau = \tau_0 + \mu_p \left|\dot{\gamma}\right|, \tag{2.2}$$

where τ is the shear stress, τ_0 is the yield stress threshold, μ_p is the plastic viscosity, and $\dot{\gamma}$ is the shear rate.

2.4.2 Herschel-Bulkley model

The Herschel-Bulkley model is particularly useful for materials like concrete that exhibit non-Newtonian behavior, meaning their flow properties depend on the applied stress. This model

describes the relationship between stress and strain rate, taking into account parameters such as yield stress, consistency coefficient, and flow behavior index [25]. The flow curve describing the behavior of this model can also be seen in Figure 2.4. Its corresponding equation is written as

$$\mu = \begin{cases} \tau_0 \dot{\gamma_0}^{-1} + k\dot{\gamma_0}^{n-1}, & |\dot{\gamma}| < \dot{\gamma_0} \\ \tau_0 \left|\dot{\gamma}\right|^{-1} + k \left|\dot{\gamma}\right|^{n-1}, & |\dot{\gamma}| \geq \dot{\gamma_0} \end{cases}, \tag{2.3}$$

where μ is the viscosity, τ_0 is the yield stress threshold, $\dot{\gamma}_0$ is the critical shear rate, k is the consistency index, n is the power-law coefficient, and $\dot{\gamma}$ is the shear rate,.

The Herschel-Bulkley model also describes the shear stress as

$$\tau = \begin{cases} \dot{\gamma} = 0, & |\tau| < \tau_0 \\ \tau_0 + k \left|\dot{\gamma}\right|^n, & |\tau| \geq \tau_0 \end{cases}, \tag{2.4}$$

where τ is the shear stress, $\dot{\gamma}$ is the shear rate, τ_0 is the yield stress threshold, k is the consistency index, and n is the power-law coefficient.

2.4.3 Roussel model

The Roussel model is another material model used in the study of concrete mixtures. This model is based on the concept of a Herschel-Bulkley type fluid but incorporates additional parameters like exponential term to represent the shear thinning behavior more accurately. This model offers a more refined characterization of concrete's non-linear behavior under various flow conditions, making it valuable for optimizing mix designs and ensuring successful concrete applications [24]. It provides an explicit framework for describing thixotropic behavior, including the material's ability to change viscosity over time and under varying stress conditions. By incorporating additional parameters that account for viscosity recovery and time-dependent behavior, Roussel's model enhances its ability to accurately predict and analyze the dynamic responses of thixotropic materials in engineering [4]. Its corresponding equation is written as

$$\mu = \tau_0 \left|\dot{\gamma}\right|^{-1} + \mu_p, \tag{2.5}$$

where μ is the viscosity, τ_0 is the yield stress threshold, $\dot{\gamma}$ is the shear rate, and μ_p is the plastic viscosity.

The Roussel model also describes the shear stress as

$$\tau = (1 + \lambda)\tau_0 + \mu_p \left|\dot{\gamma}\right|, \tag{2.6}$$

where τ is the shear stress, λ is flocculation state of the material, τ_0 is the yield stress threshold, μ_p is the plastic viscosity, and $\dot{\gamma}$ is the shear rate.

2.5 Thixotropy

Thixotropy is a rheological phenomenon that describes the ability of certain materials to change viscosity over time or under mechanical stress. Thixotropic materials lose viscosity under constant stress and regain it after the stress is removed. In Figure 2.5 there can be seen the behavior of the thixotropic fluid, specifically the dependence of shear stress on shear rate.

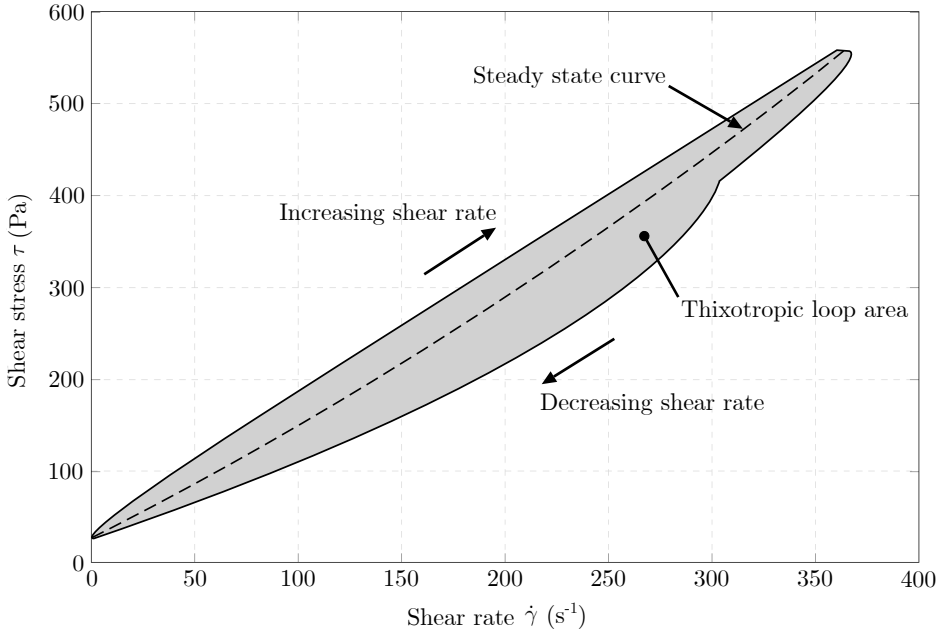

Figure 2.5: Example of the thixotropic loop of cement paste submitted to increasing and decreasing shear rate [4].

In the applications of cementitious materials like cement mortar or concrete, thixotropy is important for the proper processing and application of these materials. The thixotropic properties of cementitious mixes facilitate easy mixing and application during construction. The viscosity decreases during the application, making spreading or pouring easier. After application, the viscosity increases again, helping the material retain its shape and prevent deformations. Thixotropy also helps prevent segregation and bleeding of concrete mixes by increasing their cohesion and stability. With these properties, thixotropic cementitious materials can better fill voids and spread evenly without creating voids or uneven areas [4, 5].

2.5.1 Concrete admixtures used for modifying thixotropy

SCC needs additional admixtures in comparison with standard concrete mixes to reach its desired thixotropy. The most used admixtures are MK, Sepiolite, and nano clays. The addition of either of these materials to the SCC mix improves the thixotropic behavior and enhances its other properties. Out of these three admixtures, MK is probably the most affordable [6–8].

MK is a highly reactive pozzolanic material that is produced by calcining kaolinite. MK

is used as a partial cement replacement in high-performance, high-strength, fiber-reinforced, lightweight, precast concrete materials, and mortars. MK is added to concrete to increase compressive and flexural strengths, resistance to chemical attack, dynamic modulus of elasticity, and durability. The use of MK in concrete mixtures also has a significant impact on workability. It improves workability by increasing the cohesion and reducing the water demand of the mixture. This means that concrete containing MK can be more fluid and easier to handle during placement and compaction [6, 26, 27].

2.6 Finite element method

The Finite element method (FEM) is a numerical technique used to solve partial differential equations by dividing a continuous problem into smaller, simpler sub-domains called finite elements. Each element is defined by nodes. The elements form a mesh, which discretizes the problem domain into a collection of interconnected nodes and elements. Within each element, equations are formulated to approximate the behavior of the system, considering material properties, boundary conditions, and applied loads. These local element equations are then assembled into a global system, represented as a matrix equation, which is solved numerically to obtain solutions at discrete points called nodes [28, 29].

Creating a mesh for a simulation involves a critical need to balance the accuracy of the calculation and computational efficiency. The level of detail in the mesh directly impacts the fidelity of the simulation results. A mesh sensitivity analysis is necessary to determine the appropriate mesh density. This involves systematically varying the mesh resolution (i.e., the number and size of elements) and observing how the results change in response. The goal is to identify a mesh resolution that provides sufficiently accurate results while minimizing computational expense. This process ensures that the simulation captures the important physical phenomena without unnecessary computational burden, thereby optimizing the efficiency and reliability of the analysis [30].

There are also other parameters that describe the quality of the mesh. The two most notable parameters that describe the quality of the mesh are skewness and aspect ratio. Skewness is defined as the difference between the shape of the cell and the shape of an equilateral cell of equivalent volume. The average skewness recommended by Ansys ranges from 0 to 0.33 with values closer to 0 being the best. Maximum skewness considered acceptable by Ansys is 0.95 [31, 32]. The aspect ratio is a measure of the stretching of a cell. The average aspect ratio recommended by Ansys is anything lesser than 5. The maximum aspect ratio considered acceptable by Ansys is 10 [32].

2.6.1 Ansys program

Ansys is a powerful software used for engineering simulation and analysis. It offers a wide range of tools for structural, fluid dynamics simulations, and others. The program is used to predict how certain models will behave under real-world conditions, allowing for virtual testing and optimization of performance. Ansys program was selected for this thesis because

of its capability of working with custom geometry models, boundary conditions, creating the custom mesh, user-defined functions, and especially the FSI in the FEM model that allowed all the models to be done.

2.7 Computational fluid dynamics

Computational fluid dynamics (CFD) is a specialized field of fluid mechanics that employs numerical methods to analyze and simulate fluid flows. Instead of relying solely on experimental testing or analytical solutions, CFD leverages computational algorithms and high-performance computing to solve complex fluid dynamics problems. The equations are discretized and solved over a computational grid (mesh) that divides the fluid domain into smaller control volumes. This allows for the prediction of fluid behavior under various conditions, including flow velocities, or pressure distributions [33].

2.7.1 Multiphase modeling methods

The VOF method is a computational technique used in fluid dynamics to simulate fluid interfaces and multiphase flows. Unlike traditional approaches that track individual fluid particles or assume continuous properties, VOF represents fluid phases using a volume fraction variable within a mesh. An example of visualized phase volume fractions can be seen in Figure 2.6 [34].

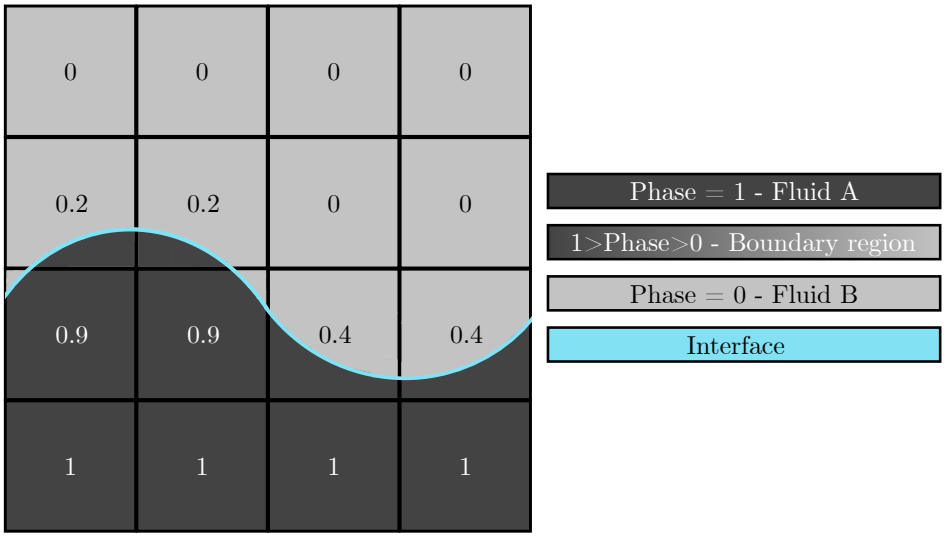

Figure 2.6: Scheme of VOF method phase volume fractions [34].

This method is particularly effective for analyzing free-surface flows and interfaces between immiscible fluids, such as air and water. VOF simulations can accurately predict fluid behavior, including fluid mixing, splashing, and wave interactions [35]. The VOF method is tracking each phase volume fraction while solving continuity and momentum equations [32]. The moment equation is defined as

$$\frac{\partial}{\partial t}(\rho\vec{v}) + \nabla \cdot (\rho\vec{v}\vec{v}) = -\nabla p + \nabla \cdot \left[\eta\left(\nabla\vec{v} + \nabla\vec{v}^{T}\right)\right] + \rho\vec{g} + \vec{F}, \tag{2.7}$$

where $\vec{v}$ is the velocity, t is the time filed, p is the static pressure, ρ is the fluid density, η is the apparent viscosity, g is the gravitational acceleration, and $\vec{F}$ is the force resulting from a sharp tension interface. The continuity equation is written as

$$\nabla \cdot \vec{v} = 0. \tag{2.8}$$

Another method used for modeling multiphase flows is the Eulerian-Eulerian method. These methods treat each flow phase as a continuum with distinct properties and model interactions between phases by averaging properties over a control volume. The phases are considered interpenetrating fluids, and separate governing equations are solved for each phase within a shared computational domain. Eulerian-Eulerian methods are computationally efficient but may require closure models for accurate interphase interaction descriptions [36].

Level-set methods are another way to model multiphase flow. The method tracks phase interfaces as the zero-level set of a higher-dimensional function. This approach efficiently captures complex and dynamic interfaces without explicit reconstruction [37].

To list a few examples, VOF can be used to model a flood that could potentially destroy a bridge [38] or to address several health-related issues [39, 40]. Many articles have dealt with SCC modeling [41–44]. Some studies are dedicated to topics closely related to the subject of this thesis, such as [45] which addresses the flow of concrete into a long wall with obstacles using a side inlet, and others [46–49].

2.7.2 Fluid-Structure Interaction

FSI involves the complex interplay between fluid flow and a deformable solid structure, where each affects the behavior of the other. In FSI simulations, the structure's deformation influences the fluid flow, and the fluid flow impacts the structure's dynamics. To simulate FSI, equations governing fluid dynamics and structural dynamics are solved simultaneously. The fluid and structural domains are discretized separately, and specialized algorithms handle their interaction at each time step [50, 51].

There are two main approaches to modeling FSI. One-way and two-way coupling. In a one-way FSI model, the fluid flow affects the structural deformation, but the deformation does not influence the fluid flow. This approach is suitable for cases where the structure is relatively rigid or the fluid forces are relatively small. In contrast, a two-way coupling FSI model considers the mutual interaction between the fluid and the structure, where both fluid and structural responses are coupled and affect each other. This method is essential for scenarios involving flexible structures or significant fluid-structure interactions. Two-way coupling requires more computational resources and sophisticated algorithms to ensure stability and accuracy in simulations, as the interactions are iteratively solved at each time step to account for the dynamic feedback between the fluid and the structure [51, 52].

To list a few examples, FSI can be used to model a situation where the bridge is flooded so that the bridge can be designed to last the flood [38] or to calculate effects of turbulent wind on a super-tall structure [53], or the heart can be modeled thanks to FSI [54]. Wings are being modeled very often using FSI [55, 56]. There are some concrete related studies such as [57, 58]. However, only a small number of studies focus on modeling SCC flow in formwork, such as [45–48], with notable work addressing the practical aspects of formwork pressures by SCC [49].

3 Applications of numerical modeling

3.1 Deflection calculation in Ansys mechanical

Reason behind this part

The initial step required was to develop a model in Ansys Mechanical to gain proficiency, as it will be essential for simulating formwork in a dedicated task aimed at evaluating the deformation caused by fresh concrete.

The subject of this FEM model was a concrete wall modeled as a simple cantilever, as creating the geometry of the wall (and then formwork) in Ansys mechanical will be needed in the next parts of the thesis.

Analytical solution

To assess whether the deflection that will be retrieved by Ansys FEM is calculated with or without any deviation it was first done by analytical solution (AS) using analytical formula. The deflection at the free end of the cantilever caused by a single force applied at the end of the cantilever can be defined as

$$w_{AS} = \frac{FL^3}{3EI}, \tag{3.1}$$

where F is the edge force at the free end of the cantilever, L is the length of the cantilever, E is the Young's modulus of the material, and I is the moment of inertia.

Information about model

To provide Ansys calculation (AC) of the deflection at the end of the cantilever w_{AC}, the model of the cantilever was modeled using FEM representing a concrete wall. It was created with dimensions of width $W = 200$ mm, length $L = 2800$ mm, and thickness $T = 1$ mm. This model was calculated as a 2D plain stress task. Fixed support was modeled on the bottom side of the model. The only load modeled was force $F = 50$ N set to the top edge of the model. Both model geometry and boundary conditions that were created can be seen in Figure 3.1a. The material model was defined with isotropic elasticity, assuming concrete as a material, Young's modulus was set to $E = 25$ GPa and Poisson's ratio to 0.2.

The mesh was chosen to be constructed using quadrilateral elements as it fits the rectangular model the best. Elements PLANE182 [59] were chosen by Ansys analysis for the calculation. This element is used to model 2D solid structures. The element comprises four nodes, with each node having two degrees of freedom, which are translations in the nodal x and y directions. The element has plasticity, hyperelasticity, stress stiffening, large deflection, and large strain capabilities support [59]. Elements used for the force application on the edge were chosen automatically by Ansys analysis as element SURF153 [59]. This element is used in load and surface effects applications. It may be assigned to the face of any 2-D structural solid element [59]. The size of each element was set to 25 mm, as this dimension fits 8 elements

in the width of the wall, which seems small enough for the size of this calculations geometry and at the same time not being too small which would slow the process of calculation and not get the results any better. The mesh element size was further refined to 10 mm near the fixed support, as seen in Figure 3.1a, to accurately calculate deflection and normal stress in this critical spot.

Results and discussion

Deflection at the end of the cantilever solved by AC was w_{AC}= 22.02 mm as shown in Figure 3.1b. The deflection retrieved by AS using Equation 3.1 was w_{AS} = 21.95 mm. This means that the AC error compared to the AS is in this case 0.3 % which is a very small deviation.

In Figure 3.1c there can be seen normal stress calculated in Ansys mechanical which can easily tell where within the proposed mesh compression and tension are in the model.

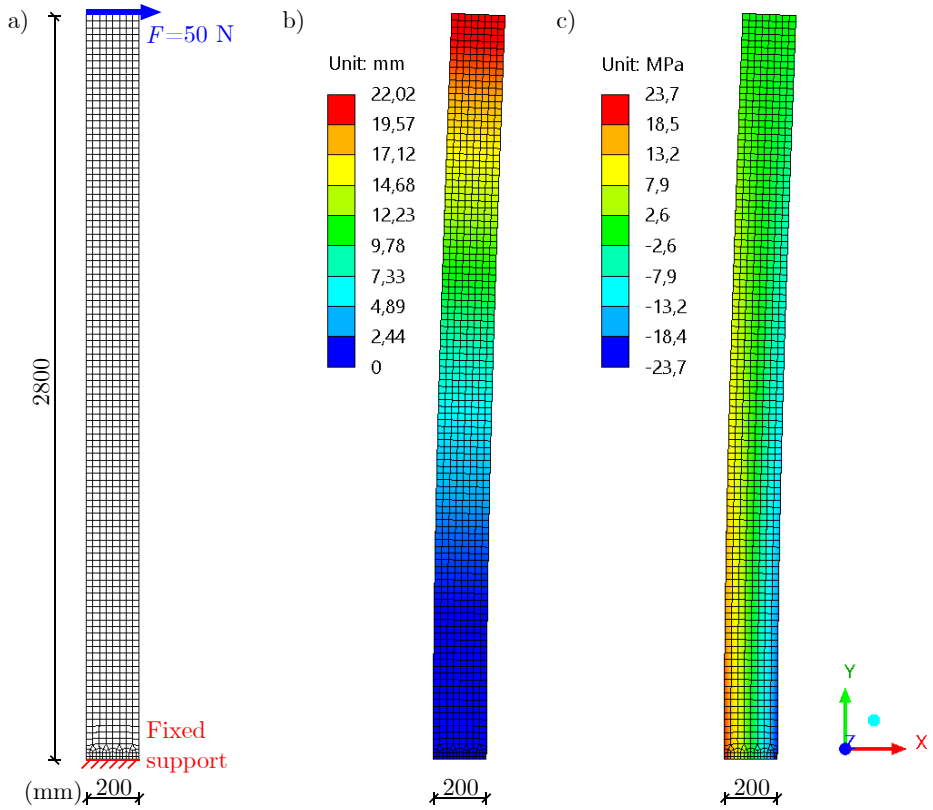

Figure 3.1: a) The geometry of the cantilever with displayed mesh and boundary conditions, b) directional deformation (X-axis), c) normal stress (Y-axis).

3.2 Fluid flow in Ansys fluent

3.2.1 Ansys example

Reason behind this part

To learn how to create geometry and mesh in Ansys SpaceClaim and how to work with fluids (primarily water and air) in Ansys Fluent, the Ansys tutorial example filling the water tank with water [32] was replicated. In this example, there were also various fluid flow settings in Ansys Fluent, such as the VOF model or inlet and outlet boundary conditions. These settings are necessary for accurately simulating the concrete flow. The example provides the necessary insight into geometry modeling and fluid flow required for the task.

Information about model

The model geometry was created with dimensions corresponding to the original Ansys example [32], shown in Figure 3.2. Mesh was modeled using quadrilateral elements with the element size set to 1 mm as followed in Figure 3.2.

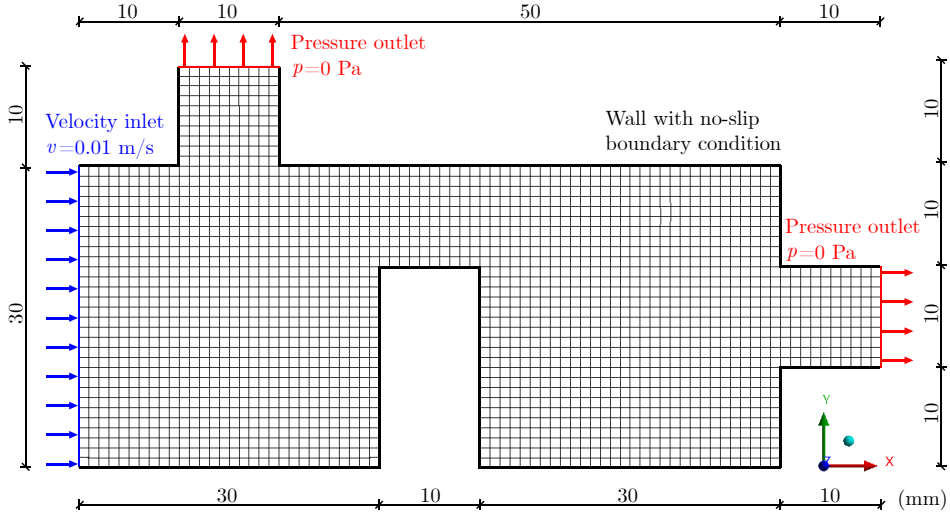

Figure 3.2: Dimensions, mesh and boundary conditions of Ansys example model.

The inlet was modeled on the left side of the model, as seen in Figure 3.2 represented with blue arrows. At the inlet, the velocity of water was prescribed as $v = 0.01$ m/s and letting only the water to flow into the model. Two outlets were modeled, one on the right side of the model and the second one on the upper side of the model. Both outlets can be seen in Figure 3.2 represented as red arrows. Both outlets were set as pressure outlets with pressure prescribed as $p = 0$ Pa. Both outlets can let both water and air out of the model, however, the upper one is primarily modeled for air to properly flow out of the model and the right one is modeled for water to properly flow out of the model. Every other edge was modeled as a wall with no-slip boundary condition, as seen in Figure 3.2 as a bold black line.

The multiphase model was set as a VOF model with two phases, water and air. The surface tension coefficient between the phases was set as 0.072 N/m. The air was modeled

with density $\rho = 1.225$ kg/m^3 and viscosity $\mu = 1.7894$e-05 kg/m·s as Newtonian fluid. Water was modeled with density $\rho = 998.2$ kg/m^3 and viscosity $\mu = 1.003$e-03 kg/m·s also as Newtonian fluid. In the initial step, a default water volume of $30 \times 15 \times 1$ mm^3 was set in the model, as depicted in Figure 3.3a. This decision was made to fasten the filling process and to enhance the progression of water flow towards the right section of the tank.

Results and discussion

The model reconstructed behaved similarly to the water flow pattern observed in the original Ansys example [32]. In Figure 3.3a there can be seen the model in step $t = 0.01$ s showing the initial state of the flow. In the Figure 3.3b there can be seen step in $t = 1.00$ s where the water already filled the left part of the model and slowly starts to overflow to the right part of the model. In Figure 3.3c there can be seen model in step $t = 2.25$ s where water shows its turbulent behavior slowly starting to fill up the right part of the model. In Figure 3.3d there can be seen model in step $t = 4.50$ s where water already filled the lower part of the right side of the model and flows to the outlet on the right side. Water has become calmer, exhibiting rather laminar behavior.

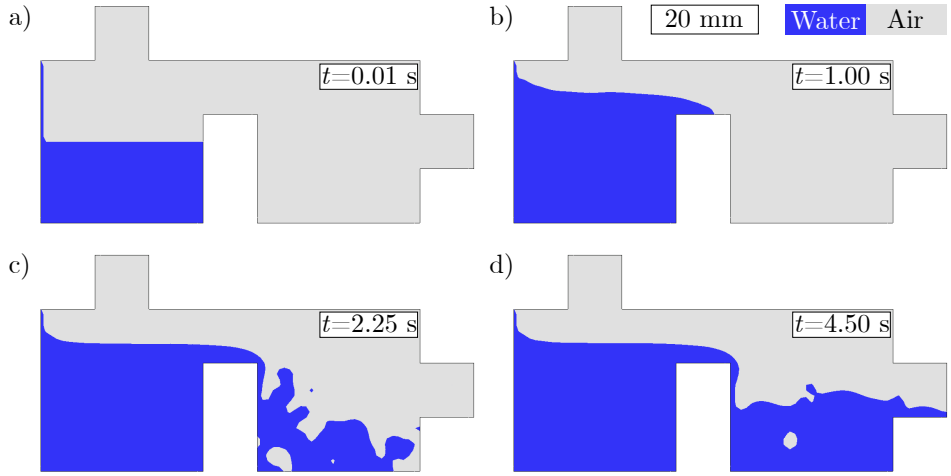

Figure 3.3: Filling the Ansys example tank model with water shown in different time steps a) $t = 0.01$ s, b) $t = 1.00$ s, c) $t = 2.25$ s, d) $t = 4.50$ s.

3.3 Behavior of fresh cement pastes

3.3.1 Slump flow test

Reason behind this part

The main objective was to learn the basics of the VOF method using a non-Newtonian fluid model, to study various cement mixes modeled using the Herschel-Bulkley model to model viscosity and to identify the influence of various parameters of the model on the flow of the mixture.

Reproduction of the slump flow test was chosen to learn and utilize the usage of the model of non-Newtonian fluid. Two cement pastes with different consistency were chosen to be calculated and compared with the experiment.

Information about model

The geometry of the model was set as shown in Figure 3.4a. The geometry corresponds to the geometry of the Hagermann mini-cone flow test (defined in ASTM C230) [10].

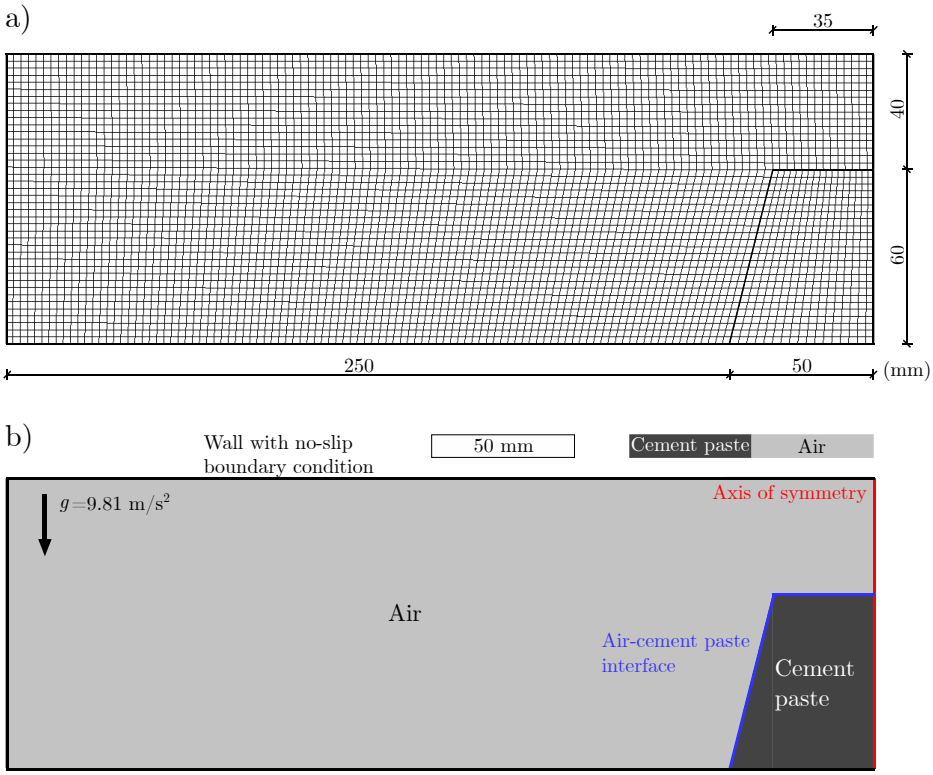

Figure 3.4: a) Geometry and mesh of the slump flow test model, b) boundary conditions of the slump flow test model.

Mesh was created with a size of each element of 2.5 mm as shown in Figure 3.4a. Considering other notable parameters of the mesh quality, the skewness of the mesh in this model is 0.05 and the aspect ratio is 1.06. As the values recommended by Ansys are from 0 to 0.33 for the skewness and values lesser than 5 for the aspect ratio, the mesh created in this model is suitable for the calculation.

In this model, the axis of symmetry was set as the right wall of the model as shown in Figure 3.4 as a red line. The cone walls are modeled as an air-cement paste interface, that disappears instantly at $t = 0$ s, allowing the spread of the paste. Every other wall in the model is modeled as a wall with no-slip boundary condition. In the model there is also gravitational acceleration applied, $g = 9.81$ m/s^2.

The VOF model with the laminar flow was used to model fluids in this model. The air was modeled with density $\rho = 1.225$ kg/m^3 and viscosity $\mu = 1.7894$e-05 kg/m·s as Newtonian fluid. The fluid model for the cement pastes was selected to be the Herschel-Bulkley as it

reliably describes the behavior of the concrete flow. Two cement pastes based on Portland cement CEM I-42.5 R (Českomoravský cement) were chosen. Cement paste A has 1 % of MK Mefisto L05 used as an admixture with no plasticizers added, and water-cement ratio w/c 0.40. Cement paste B has water-cement factor w/c 0.45 with no admixtures. The density of both pastes is $\rho = 1800$ kg/m^3. These two cement pastes were chosen deliberately to have a different spread and therefore flow behavior. Cement paste is set in the model as seen in Figure 3.4b.

Results and discussion

In Figure 3.5, the results of the Ansys calculation for cement paste A at various time steps can be seen. The model successfully describes the real behavior visible in the experiment as seen in Figure 3.6.

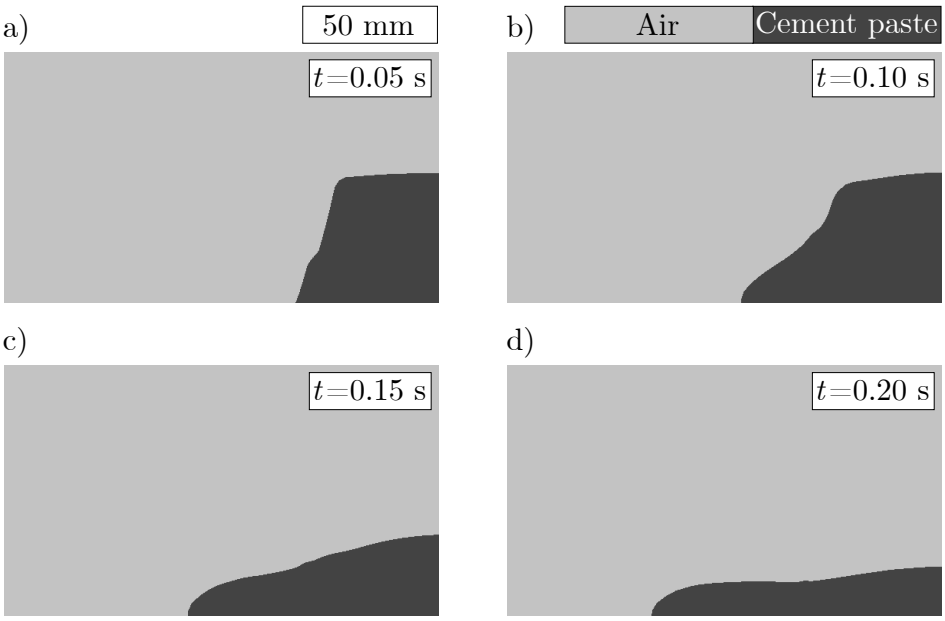

Figure 3.5: The results of slump flow test simulation for cement paste A shown in different time steps a) $t = 0.05$ s, b) $t = 0.10$ s, c) $t = 0.15$ s, and d) $t = 0.20$ s.

The parameters of the Herschel-Bulkley model were chosen by iteration of individual parameters to represent the real spread of the pastes from the experiment. The parameters were chosen as can be seen in Table 3.1.

Table 3.1: Herschel-Bulkley model parameters of cement pastes.

	τ_0 (Pa)	k (Pa·s^n)	n (-)	$\dot{\gamma}_0$ (s^{-1})
Cement paste A	19.36	8.63	0.44	0.48
Cement paste B	85.58	17.63	0.52	0.59

It is clear that in cement paste B, τ_0 is 4.4 times greater than in cement paste A and k in cement paste B is 2 times greater compared to cement paste A, indicating that these parameters exert the greatest influence on the final spread. Based on the resulting parameters

corresponding to the real experiment can be seen that the lesser the value of either of these two parameters is, the higher the final spread. It can also be deduced from Table 3.1 that parameters n and $\dot{\gamma}_0$ do not have this much influence on the final spread. However, they operate similarly to the other two parameters, indicating that the lower the value of either parameter, the greater the final spread.

For cement paste A, the final spread from Ansys calculation is 109.5 mm, and the final spread from the experimental data is 107.5 mm. The height of the slump from the Ansys calculation is 9.3 mm, and the height of the slump from the experimental data is 10.0 mm. In comparison, the final spread results are 98 % same, and the height of the slump results are 93 % same. Visual comparison of the results can be seen in Figure 3.6a.

For cement paste B, the final spread from Ansys calculation is 74.2 mm, and the final spread from the experimental data is 75.0 mm. The height of the slump from the Ansys calculation is 27.8 mm, and the height of the slump from the experimental data is 27.2 mm. In comparison, the final spread results are 99 % same, and the height of the slump results are 98 % same. Visual comparison of the results can be seen in Figure 3.6b.

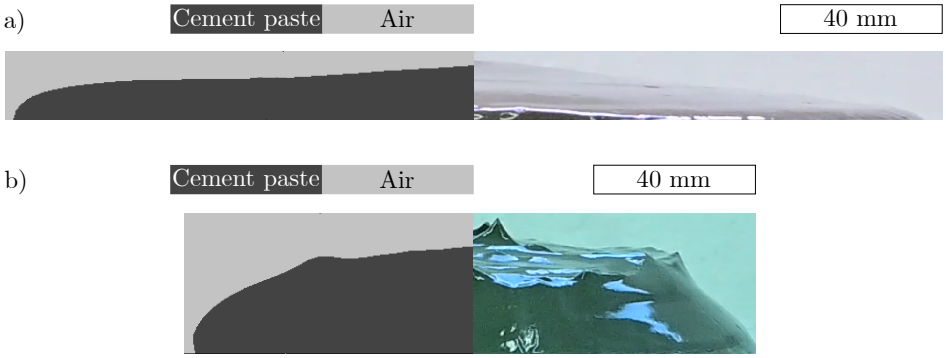

Figure 3.6: Slump flow test final spread comparing Ansys calculation with experimental data for a) cement paste A, b) cement paste B.

Based on both of these comparisons it can be said that Ansys calculation of the spread corresponds to the real experiment indicating the appropriate parameters were chosen to represent both cement pastes.

3.4 Flow of concrete into the wall

The main objective of this section is to create a model of the wall to calculate the pressure on the formwork during the filling of the wall with SCC. This task was further divided into sub-tasks to address each part individually.

This section limits the wall height of models to 2.8 m because most in-situ experiments were performed on standard-size walls. Additionally, filling taller walls could lead to instability in the calculations since the Herschel-Bulkley model is only supported with laminar flow in the Ansys program. Thus, the model requires implementing moving inlet boundary conditions or filling the wall with multiple inlets, which are gradually activated and deactivated.

3.4.1 Selection of boundary conditions for wall models

Reason behind this part

The first sub-task was to fill the wall with fresh concrete without any structural interaction. Three different boundary conditions were tested to determine the most effective filling method for the wall.

Information about model

Three 2D transversal sections of the wall models were created with identical measures of the wall itself. The width of the model domain was 200 mm and the height was 2900 mm, where 2800 mm represents the height of the wall. The remaining 100 mm was intentionally left as empty space between the formwork. Then, these models were divided by whichever inlet was added to them. These dimensions correspond to the average wall measures. All three models can be seen in Figure 3.7. In the whole model domain of all three models, there is also gravitational acceleration applied, $g = 9.81$ m/s^2.

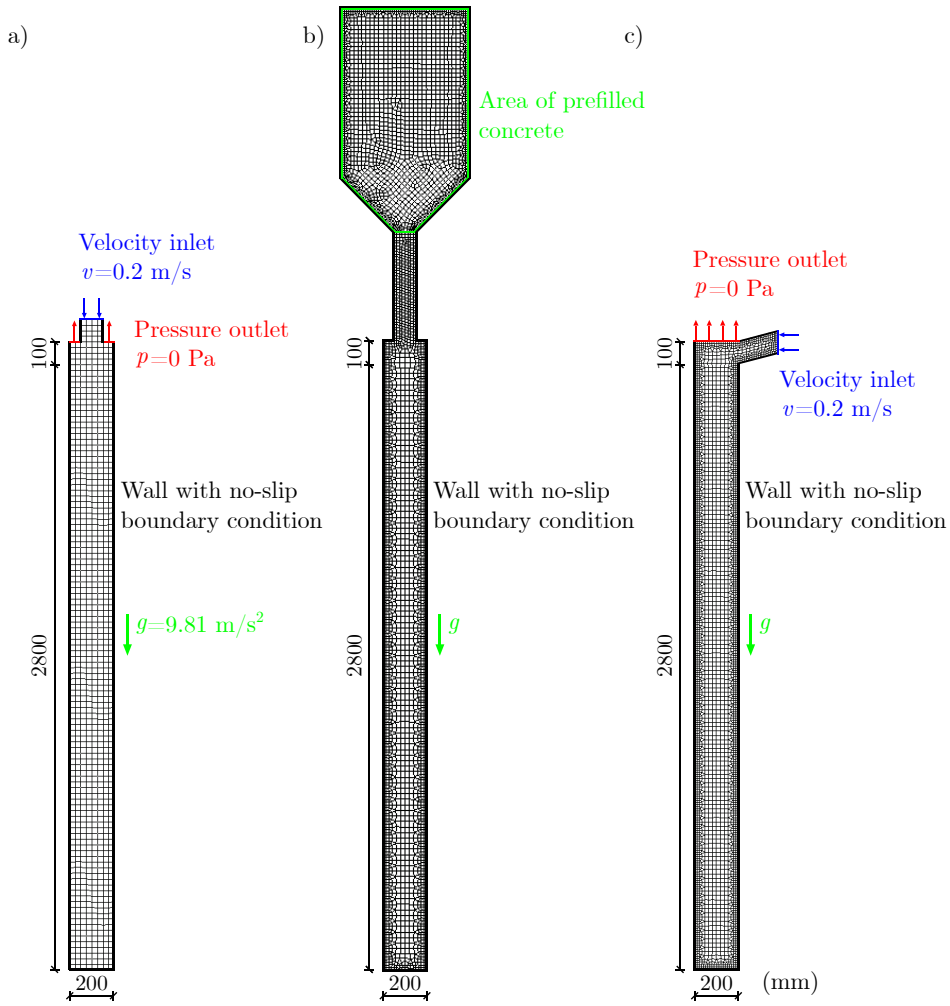

Figure 3.7: Geometry and boundary conditions of a) top-inlet model, b) silo model, c) side-inlet model.

The first, the top-inlet model, was created with one inlet and two outlet boundary conditions on the top of the wall. The top edge is set as an inlet with a flow velocity of 0.2 m/s, letting only the concrete flow in. Then, two walls are going down from the corners of the inlet, representing the walls of the sleeve. The other two top parts of the wall model are set as outlets for the escaping air where pressure 0 Pa needs to be overcome. The rest of the wall edges were prescribed no-slip boundary conditions. The mesh of the model domain was filled with quadrilateral elements, the size of which was set to 25 mm. The mesh and geometry of the model can be seen in Figure 3.7a.

The second, the silo model, was modeled without inlet and outlet and had a tank on the top of the wall prefilled with concrete from which the concrete flows through the sleeve to the wall. The geometry of this model can be seen in Figure 3.7b. The mesh in this model was divided into two parts. In the wall and sleeve parts of the model, the elements were modeled using quadrilateral elements with the size of one element set as 25 mm. In the silo part of the model, the elements were modeled as quadrilateral with the size of one element set as 20 mm. Both the sizes were further refined near every wall in the model.

The third, the side-inlet model, was very similar to the first top-inlet model. The main difference is the inlet in this model is modeled on the right side of the top part of the model. The main reason was the model allowed concrete to flow on the side of the wall instead of directly falling through the domain. However, it does not reflect the actual sleeve dimensions as the top-inlet model. The setup of boundary condition values is the same as for the top-inlet model. The mesh in the model was modeled using quadrilateral elements with the size of one element set as 20 mm. This size was further refined near every wall in the model. The model is shown in Figure 3.7c.

The VOF model with the laminar flow was used to model fluids in these models. The air was modeled with density $\rho = 1.225$ kg/m^3 and viscosity $\mu = 1.7894\text{e-}05$ kg/m·s as Newtonian fluid. The concrete flowing in all these models was modeled as a user-defined function corresponding to the Herschel-Bulkley model. The user-defined function enables additional material implementation to the Ansys software, such as the Rousell model [24], which captures thixotropic behavior. Specific parameters for concrete viscosity are shown in Table 3.2 and for this test were taken for concrete mixture B. The density of the concrete was set as $\rho = 2400$ kg/m^3.

Table 3.2: Herschel-Bulkley model viscosity parameters of concrete mixtures.

	τ_0 (Pa)	k (Pa·s^n)	n (-)	$\dot{\gamma}_0$ (s^{-1})
Concrete mixture A	100	8	0.5	0.5
Concrete mixture B	200	8	0.5	0.5
Concrete mixture C	500	25	0.5	0.5

The SIMPLE scheme was used in this model as a pressure-velocity coupling solution method. The SIMPLE scheme is the default algorithm for solving transient simulations using pressure-based solver [32]. Adaptive time stepping was used for this calculation, as it

combines the possibility of speed of calculation with its sufficient accuracy. The first time step size and maximum time step size were set to 0.01 s, the minimum step change factor was set as 0.5, and the maximum step change factor was set as 1.5. For the top-inlet model, the total time of the calculation was set as 30 s, although the wall was filled at 27 s. A total of 9682 time steps were calculated, meaning the average time step size was 0.003 s. The wall was filled in 9620 time steps. The number of maximum iterations per time step was set as 20.

Results and discussion

In Figure 3.8, the results of all three models can be seen in the early stage of the calculation.

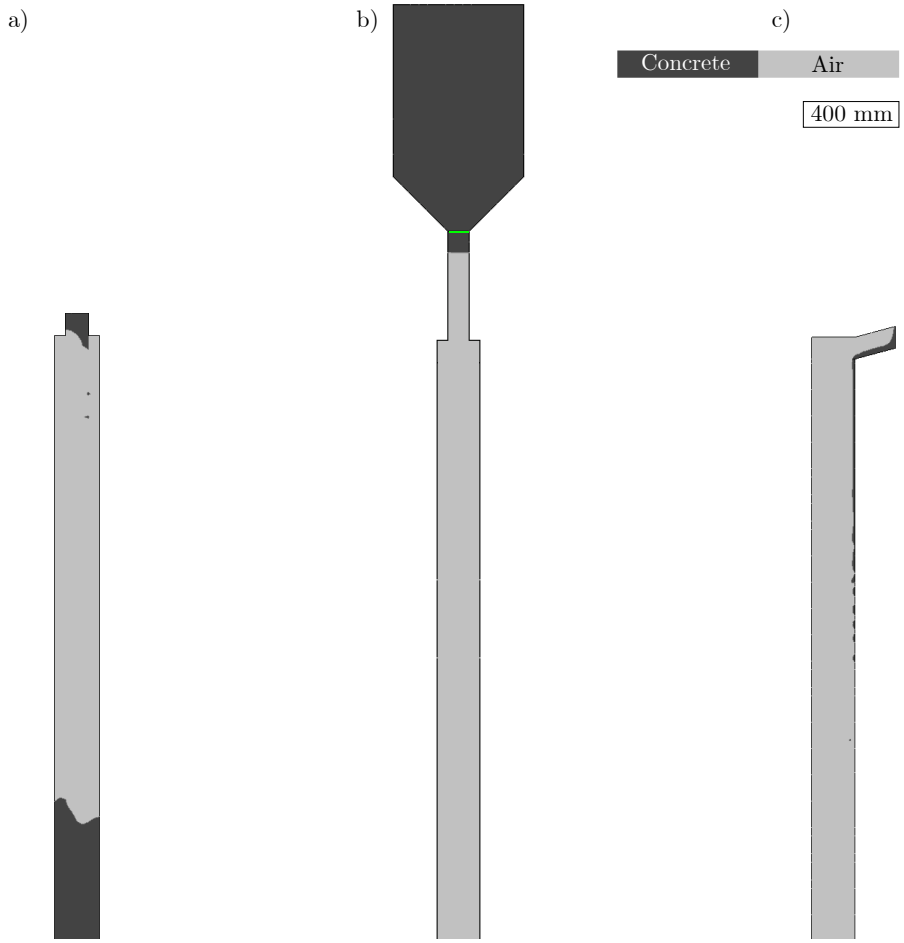

Figure 3.8: Results of the concrete flow in the early stage of calculation in a) top-inlet model, b) silo model, c) side-inlet model.

The top-inlet model exhibits a suitable flow of the wall filling up, as seen in Figure 3.8a. In Figure 3.8b, there is the silo model at the time of calculation error. The calculation failed during the first time step. One of the main issues with the silo model was probably that the model had no outlet, and therefore, the air had nowhere to escape from the domain. Then, in Figure 3.8c, there is the side-inlet model also at the time of calculation error. The issues in this model could be solved by adjusting the mesh and the time-stepping options. Even

though the side-inlet model could work if further efforts to improve the model have been made, it was abandoned because the inlet on the side of the model does not describe the flow of the concrete, so it resembles reality.

In conclusion, the top-inlet model was chosen for further use and improvements as it was the most stable of the three made models. However, both silo and side-inlet models could be made functional with further improvements, but since the top-inlet model was working as presumed. Both models were omitted for further calculations.

The more detailed results of the top-inlet model filling process are shown in Figure 3.9a–e. This model can calculate the total pressure (static pressure combined with dynamic pressure) in the concrete itself, as seen in Figure 3.9f, but not the real stress on the walls representing the formwork. However, the calculated pressure can be further used in structural analysis to calculate the actual pressure on the formwork. The goal accomplished in this model is that the estimated visual quality of the faced concrete can be recognized from the flow figures or the animation of the flow. The model depicts the flow of concrete as it would occur in reality. Initially, when the concrete falls from a great height, it appears to roll, but as the mixture accumulates, it becomes calmer. In the final Figure 3.9e, a filled wall is shown, indicating almost no air pockets, demonstrating the suitability of this mixture for use as faced concrete.

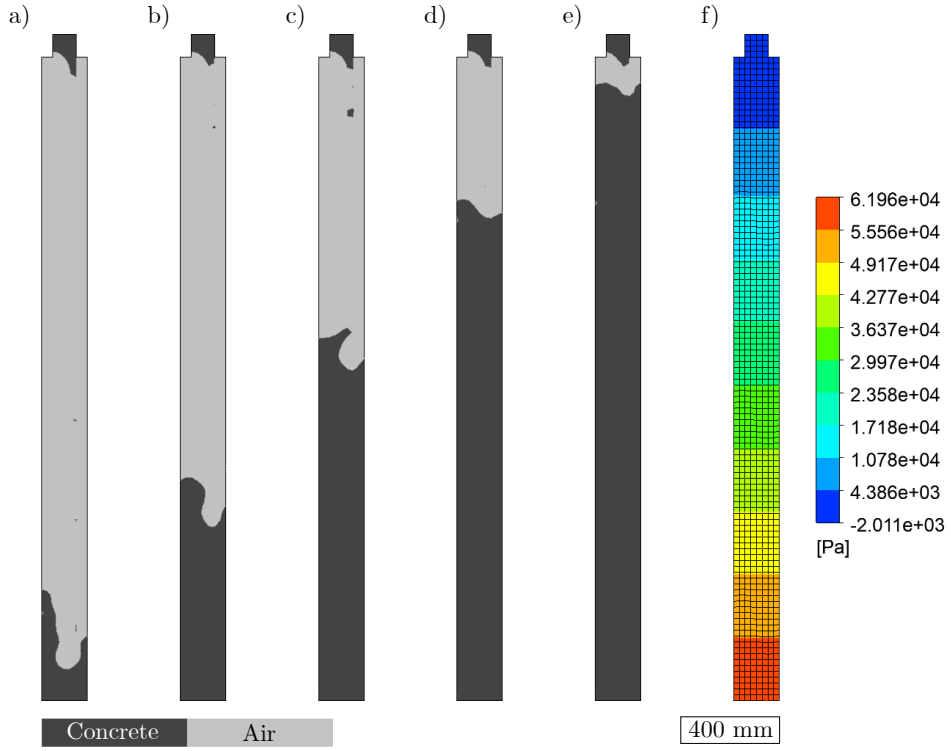

Figure 3.9: 2D model of the wall showing the flow of concrete mixture A in different time steps a) $t = 4$ s, b) $t = 10$ s, c) $t = 16$ s, d) $t = 22$ s, e) $t = 27$ s, f) total pressure in the concrete in $t = 27$ s.

3.4.2 Side view of wall filling

Reason behind this part

To accurately capture the flow details around corners and to provide an overview of the flow, a 2D model of the longitudinal section of the wall was created.

Information about model

The geometry parameters of this model are shown in Figure 3.10a. The empty space in the model represents the window, which is a problematic part of the construction, as the concrete does not always fill the space around it.

The elements of this model mesh were created as quadrilateral with the size of elements set to 100 mm. Mesh can be seen in Figure 3.10a.

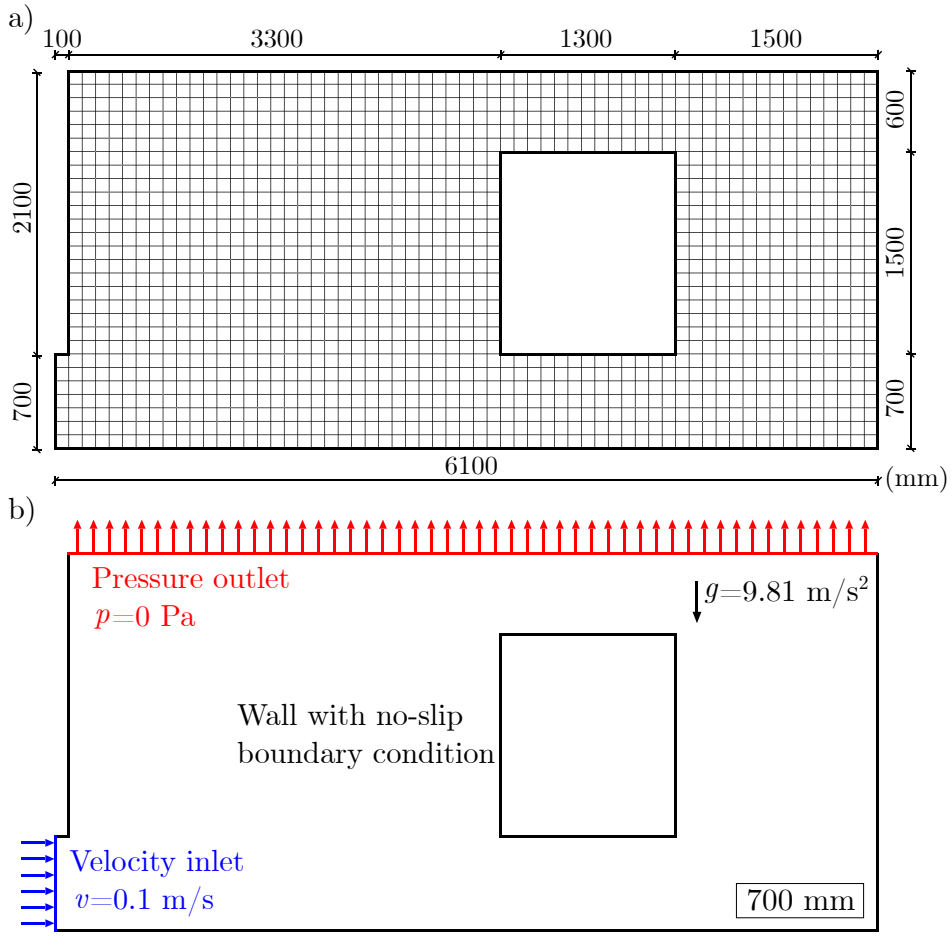

Figure 3.10: a) Geometry and mesh of the longitudinal section of the wall, the side view model, b) boundary conditions of the longitudinal section of the wall, the side view model.

The inlet and outlet are modeled as seen in Figure 3.12b with the inlet velocity set as v = 0.1 m/s. The inlet was modeled on the left side of the model to fasten the calculation and to assure the calculations stability. All other parameters in this model are set the same as in Section 3.4.1. The Herschel-Bulkley parameters for the concrete in this model are set as concrete mixture C from table 3.2. The density of the concrete was set as $\rho = 2400$ kg/m^3.

Results and discussion

This model is less stable than all previously mentioned wall models. The inlet had to be positioned at the bottom left side of the model because placing it at the top would likely result in calculation errors. Although this inlet placement aids the calculation process, it pushes the concrete to the right of the model, causing unrealistic and unsuitable behavior of the mixture. The calculation for this model takes too long and does not provide significantly more results than the previous model. Due to time constraints, the model has not been further improved after successfully demonstrating the desired effect of flow around the window. Figure 3.11 shows the flow of the concrete at different time steps.

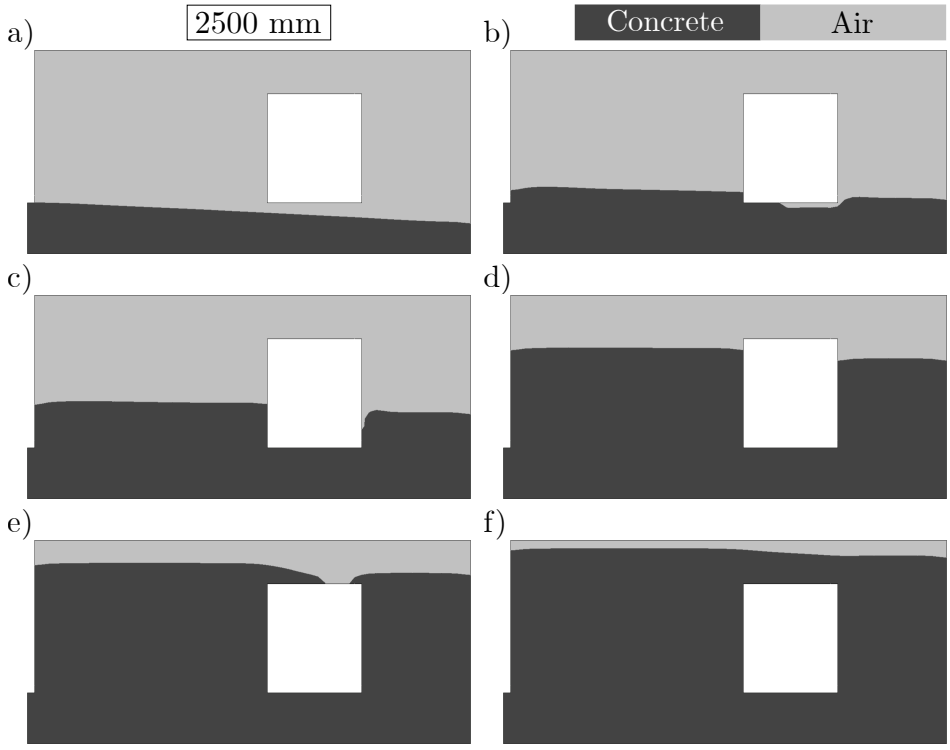

Figure 3.11: 2D model of the longitudinal section of the wall, the side view model, showing flow of concrete mixture C in different time steps a) t = 50 s, b) t = 70 s, c) t = 100 s, d) t = 150 s, e) t = 180 s, f) t = 200 s.

In Figure 3.11b, an air pocket can be seen under the window. With the inlet at the bottom left side of the model, this is a relatively acceptable example, because the air pocket gets filled pretty soon after this moment, but if the inlet was at the top of the model, the air pocket would be much larger. Figure 3.11c shows the concrete being pushed to the right side of the model. This is due to two reasons: firstly, the inlet pushes the concrete too much from the left side of the model to the right, which is incorrect. Secondly, the absence of mixture aging and thixotropy would prevent the solidification of the mixture, which would flow out of the area. Figure 3.11e shows the concrete gradually touching both sides of the window, overflowing on the top of it from the left side and being pushed out from the right side onto the window.

This model cannot display the visual quality of faced concrete, as the inlet constantly pushes the concrete across the model, filling out the air pockets. The improved model should take into account a better material model and the use of a moving inlet.

3.4.3 Concrete flow into the formwork

Reason behind this part

In this task, all previous sub-tasks were combined to create a 3D model of a wall concrete filling with one-way FSI to calculate pressure on the formwork.

Information about model

The model was created as a 3D task since the pressure calculated in Fluid Fluent cannot be applied on the edge of the structure as a boundary condition, but the face needs to be used. However, to reduce the calculation demand of the task, the thickness of the wall was set as 25 mm, which corresponds to the width of one quadrilateral element. Such a simplification enables the creation of a 2D task using 3D elements. The wall was modeled as 200 mm in width and 3000 mm in height. The wall itself was assumed to be 2800 mm in height, and the remaining 200 mm was left empty. Both parts of the formwork were 100 mm wide and 3000 mm in height. The other parts of the model domain served to give the formwork space to deform. The front view of the model with the geometry is shown in Figure 3.12a.

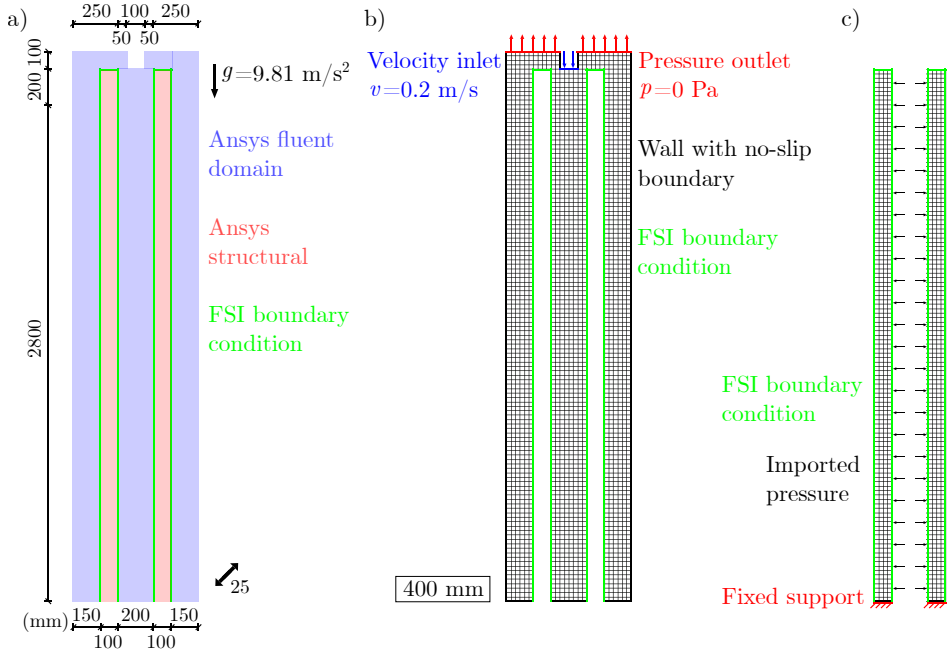

Figure 3.12: a) Geometry and boundary conditions of the 3D wall-filling model with formwork, b) boundary conditions of Ansys fluent part of the model, c) boundary conditions of Ansys structural part of the model.

The mesh elements of both parts, Ansys fluent and Ansys structural, were created as quadrilateral, with the size of the elements set to 25 mm. In Ansys structural, elements

SOLID186 [59] were chosen by Ansys analysis for the calculation. This element is a higher order 3D 20-node solid type of element, with each node having three degrees of freedom per node [59]. Mesh can be seen in Figure 3.12b–c for both parts of the model. The inlet and outlets are modeled as seen in Figure 3.12b with the same parameters set as in Section 3.4.1. The front and back walls were set as symmetry planes to capture only the cutout of part of the wall. The edges between the formwork and the interface are modeled as FSI boundary conditions for the model to be able to transfer the pressure calculated in the Ansys fluent from the selected faces to the formwork modeled in Ansys mechanical, where the selected faces correspond to those in Ansys fluent and to calculate its deformation and stress. The formwork was modeled as isotropic elastic with Young's modulus set to $E = 60$ GPa and Poisson's ratio set to 0.3. Fixed support was modeled on the bottom face of both formwork parts.

The simulation scheme and time-stepping setting were the same as in Section 3.4.1. A total of 10680 time steps of the flow were calculated in Ansys fluent. Calculation in Ansys structural was done in 1 time step.

Results and discussion

In Ansys results, an animation of the volume fraction of the whole wall-filling process was made for all concrete mixtures.

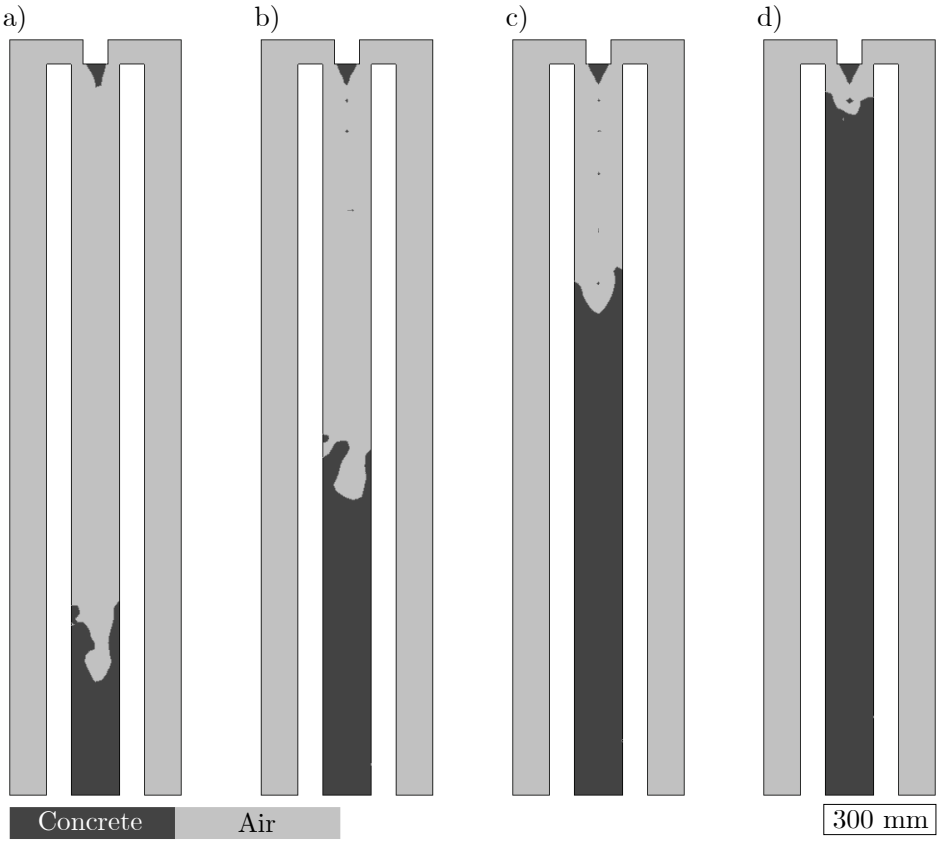

Figure 3.13: 3D wall-filling model with formwork showing concrete mixture A flow in different time steps a) $t = 7$ s, b) $t = 14$ s, c) $t = 21$ s, d) $t = 28$ s.

Four animation frames were chosen to show the flow process of concrete mixture A, as visible in Figure 3.13, showing the surface quality of the faced concrete can be recognized from this model.

In Figure 3.14, all three concrete mixtures (A, B, and C) can be seen at a time when the wall is completely filled. There is a clear difference between the three mixtures, showing that the higher the τ_0 and k parameters, the worse the concrete wall's surface quality. In Figure 3.14a, where the concrete mixture A is there can be seen that the mixture is suitable for use as faced concrete since there are no air pockets. In Figure 3.14b, where the concrete mixture B is, it can be seen that with higher τ_0, the air pockets are visible in some places. In Figure 3.14c, it can be seen that concrete mixture C has significant air pockets, indicating that this mixture is not suitable for use as faced concrete.

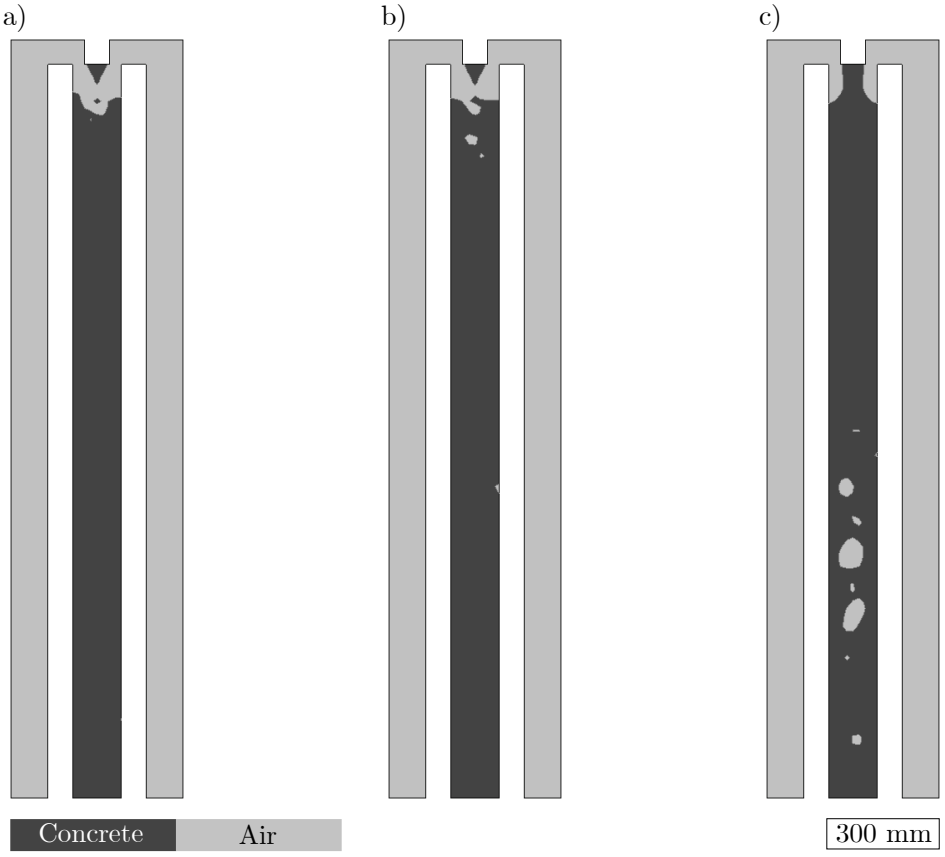

Figure 3.14: 3D wall-filling model with formwork showing visual quality at the stage of a filled wall for concrete mixtures a) A, b) B, c) C.

In Figure 3.15a, an example of a faced concrete wall with parameters approximately corresponding to concrete mixture A is shown. It is evident from the figure that there are almost no air pockets, similar to the model. Conversely, Figure 3.15b presents an example of faced concrete exhibiting a high number of air pockets. The parameters of this concrete approximately correspond to concrete mixture C. Once again, the similarity between the experimental results and the model is apparent.

This model can calculate the pressure exerted on the formwork by the fresh concrete and utilize it to compute the deformation and equivalent (von Mises) stress of the formwork. The

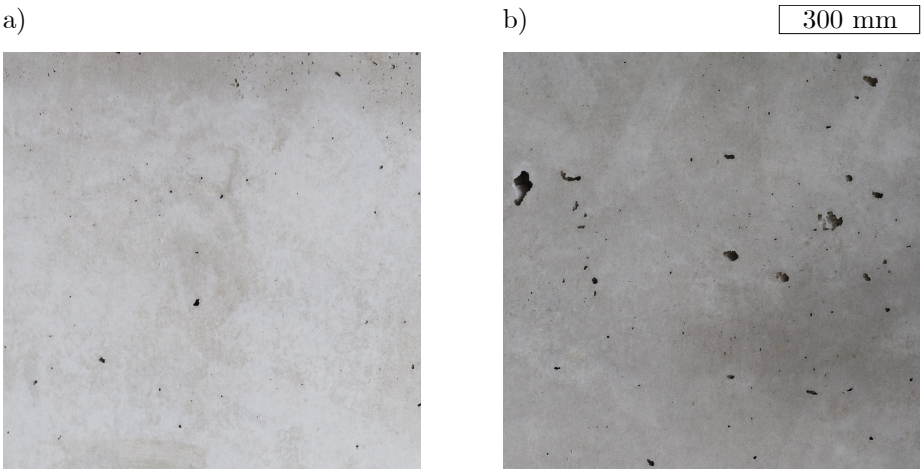

Figure 3.15: Examples of faced concrete walls in-situ with a) suitable visual surface quality, b) poor visual surface quality.

Table 3.3: Maximum values of the equivalent stress and deformation for the concrete mixtures A, B, and C.

	τ_0	Total pressure	Equivalent stress	Deformation
	(Pa)	(kPa)	(MPa)	(mm)
Concrete mixture A	100	66.32	55.33	31.4
Concrete mixture B	200	64.94	52.48	29.5
Concrete mixture C	500	59.28	53.98	31.3

maximum total pressure for each concrete mixture is listed in Table 3.3.

The total pressure in concrete mixture B drops by 2 % compared to mixture A, and the total pressure in concrete mixture C drops by 12 %, this principle corresponds to reality. However, decreasing total pressure has no significant effect on the resulting equivalent stress and deformation of the formwork. Figure 3.16 displays the equivalent stress in the formwork resulting from all three concrete mixtures. The maximum values of equivalent stress for all three concrete mixtures are summarized in Table 3.3.

However, even the change of τ_0 by 500 % did not change the total pressure by more than 12 %. In the current model, the equivalent stress exhibits a maximum deviation of 5 % across all three mixtures. This suggests that the current estimation of pressure on the formwork is inaccurate. To accurately represent the actual pressure, the model needs to incorporate the thixotropic material property and consider the aging process of the mixture. Additionally, the model should be developed as a two-way FSI instead of a one-way FSI. This approach is necessary to calculate the deformation of the formwork during the filling process and to simulate the behavior of the concrete accurately. Figure 3.17 and Figure 3.18 are showing the comparison of the calculated total pressure with in-situ experiment data. Details about experimental setup and measurement can be found in [60]. Two concrete mixtures were tested. The First of them corresponds to the concrete mixture A and is based on CEM II 42.5R (inverted Abrams cone test, slump 74.8 mm).

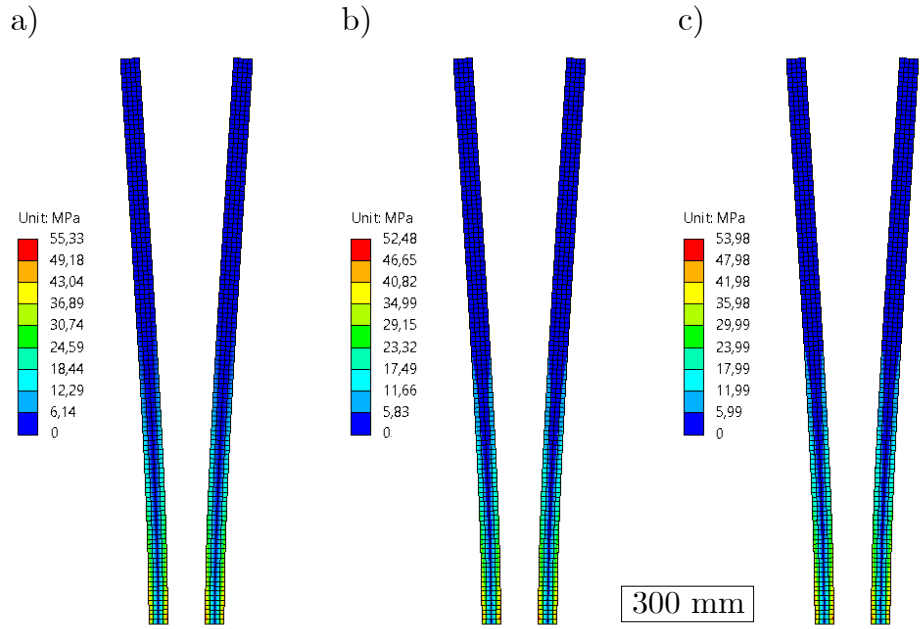

Figure 3.16: The equivalent stress in the formwork for concrete mixtures a) A, b) B, c) C.

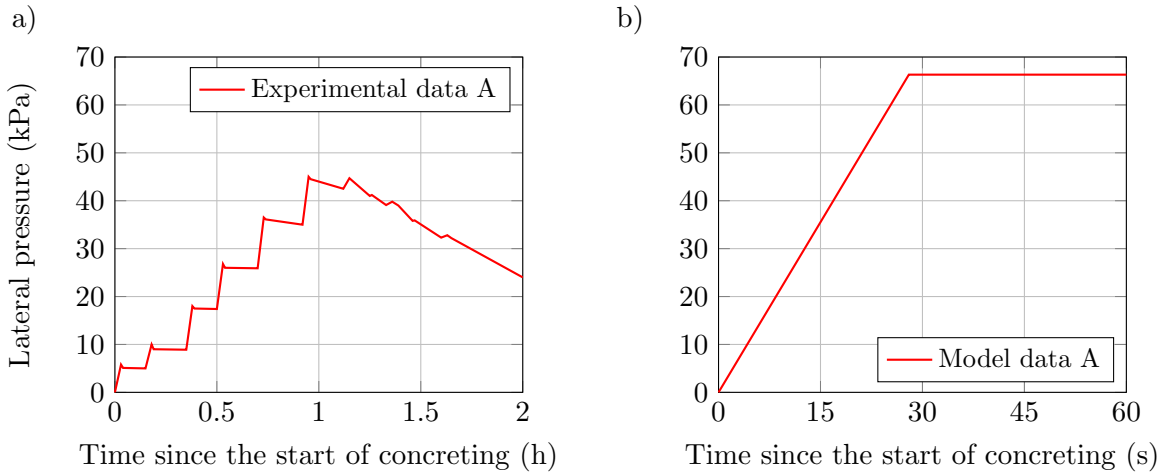

Figure 3.17: Comparison of lateral pressure of concrete mixture A established by a) experiment, b) model.

This data clearly shows that the calculated concrete flow is not close to the real filling of the formwork, as it does not represent the material aging and thixotropy which can be seen in Figure 3.17a as descending line, and the calculation does not have the stops between many parts of the filling. The maximum lateral pressure on the formwork for the concrete mixture A obtained from the experiment is 44.7 kPa, while in the model the lateral pressure is 66.3 kPa. Summarizing this, the resulting error of the computational model compared to the experiment is 48.3 %.

The second mixture corresponds to the concrete mixture C and is based on CEM II 42.5R, MK 10 %, Xseed 1.0 % (inverted Abrams cone test, slump 61.6 mm). Lateral pressure on the formwork in comparison with Concrete mixture C can be seen in Figure 3.18.

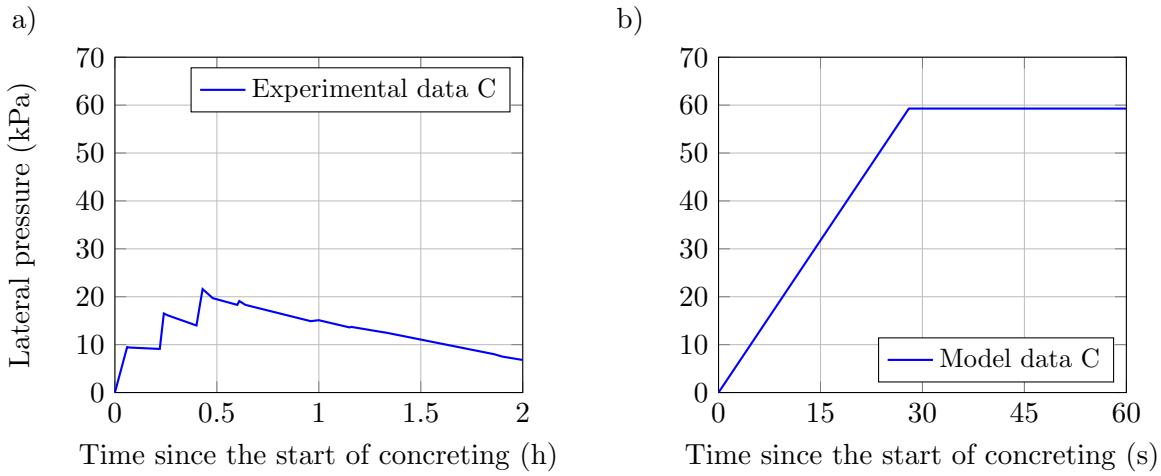

Figure 3.18: Comparison of lateral pressure of concrete mixture C established by a) experiment, b) model.

The maximum lateral pressure on the formwork for the concrete mixture C obtained from the experiment is 21.6 kPa, while in the model the lateral pressure is 59.3 kPa. Summarizing this, the resulting error of the computational model compared to the experiment is 274 %. This is worse than the results of concrete mixture A, because this mixture in the experiment was highly thixotropic, and as the thixotropy property is not implemented in the Herschel-Bulkley model, it can not be calculated correctly with this setup.

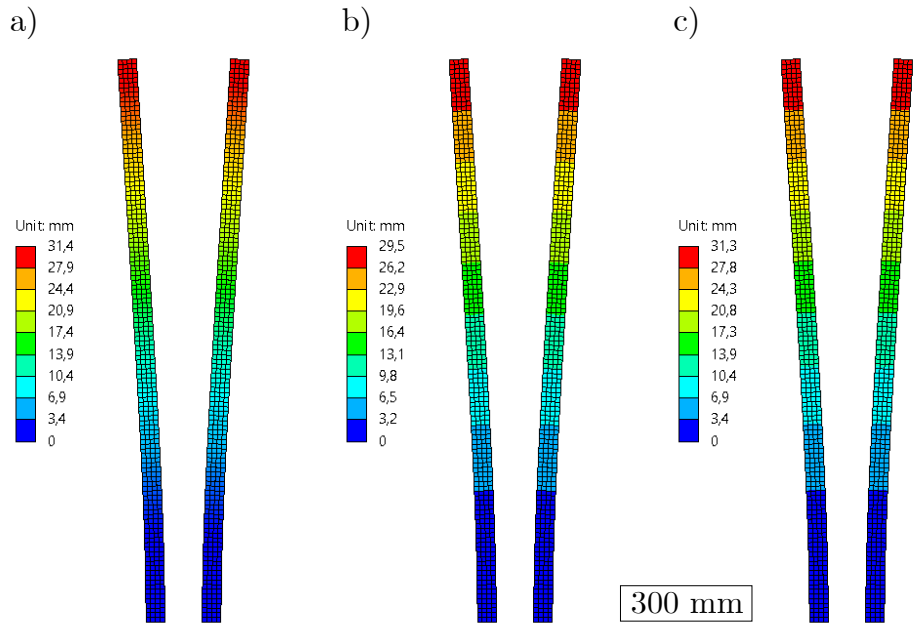

Figure 3.19: The deformation of the formwork for concrete mixtures a) A, b) B, c) C.

Another model improvement that can help calculate the pressure more precisely is the formwork static scheme. The formwork can be modeled with the correct distribution of the supports, thus remodeling the current fixed support to a pinned support, then adding another one to two supports by the height of the wall representing the support bars, and in the end,

modeling the connecting rods that are holding the two parts of the formwork together.

The deformation of the formwork has a maximum deviation of 6 % across all three mixtures, as seen in Figure 3.19. Thus the deformation of the formwork for this model gives the same conclusion as the equivalent stress results, that the model is inadequate for this calculation. The maximum values of the deformation of the formwork for all three concrete mixtures are summarized in Table 3.3.

The resulting equivalent stress versus yield stress threshold, and the resulting deformation versus the yield stress threshold are presented in Figure 3.20. The figure illustrates the minimal impact of the variation in the yield stress threshold on both the resulting equivalent stress and deformation.

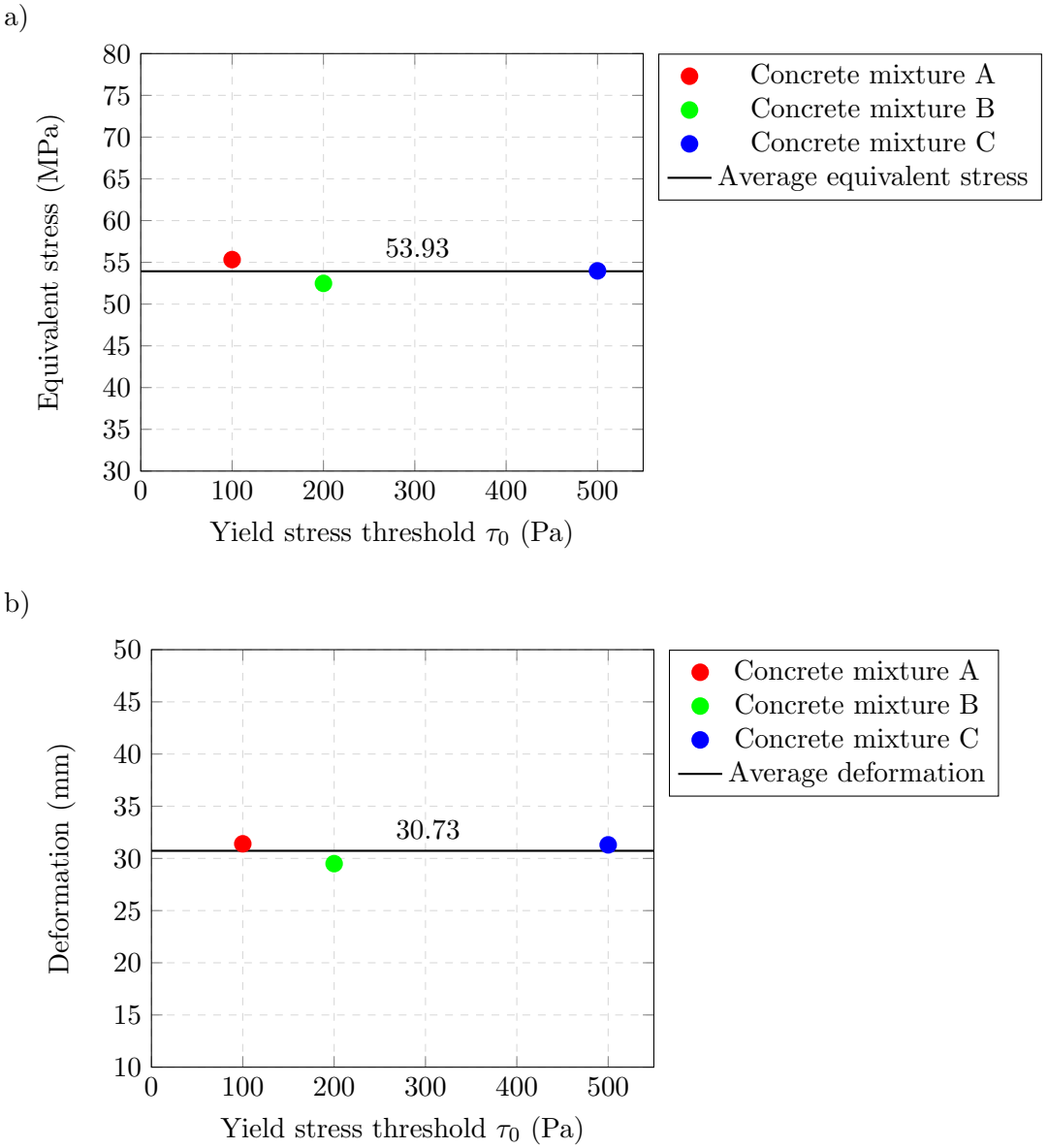

Figure 3.20: Influence of the Yield Stress threshold parameter on calculated a) equivalent stress, b) deformation of the formwork.

Currently, the wall is filled continuously because mixture aging and thixotropy are not

implemented. Once these parameters are included, there must be time for the mixture to change its properties over time, representing the re-filling of the concrete bucket.

4 Conclusions

In conclusion, this thesis investigated the numerical analysis of lateral pressures acting on the formwork and the development of corresponding models for the calculation models. Based on the calculated results, the following conclusions can be deducted:

- The slump flow test successfully demonstrated that parameters τ_0 and k have the most significant influence on the spread of the slump. For instance, increasing the value of τ_0 by 440 % and simultaneously increasing k by 200 % for cement paste B compared to paste A resulted in a 148 % increase in the spread. Conversely, parameters n and $\dot{\gamma}_0$ have negligible effects on the final spread. This insight facilitates more accurate estimation of the appropriate mixture parameters for faced concrete in future applications.

- The development of the 2D wall model revealed that the top-inlet model is the most suitable for calculations. It closely corresponds to the real-life position of the sleeve and exhibits the highest stability among the three models created.

- It was observed that as the value of τ_0 increases, the surface quality of the concrete wall deteriorates. Concrete mixtures with τ_0 values up to 100 Pa are suitable for the faced concrete. Conversely, mixtures with τ_0 values between 200–500 Pa leave a significant amount of air pockets in the poured mixture.

- The pressure on the formwork calculated in this model has a relatively suitable downward trend, but the values still do not correspond to the in-situ experiments. The higher the τ_0 is, the lower is the pressure, however, the deviation resulting from data compared between the experiment and the model is 48.3–274 %. The reason for this is the insufficiency of the model in the solidification of the mixture, which is not captured by model.

- The calculated equivalent stress and deformation together with the total pressure showed that the Herschel-Bulkley model is not appropriate for the calculation. Even though τ_0 changed by 500 %, the difference in any of these values was no more than 12 %. Therefore the thixotropy and aging of the mixture are crucial for the results close to reality.

4.1 Future outlook

This thesis found the one-way FSI method unsuitable for calculating pressures on formwork and replicating real material behavior. The current model should be further improved by:

- Using a wall-filling model with formwork using two-way FSI with system coupling method.

- Adjusting the material model that can capture thixotropy behavior and aging of the mixture, such a model is not present in Ansys software and needs to be implemented by user-defined functions.
- Adjusting the static scheme of the formwork and adding the rods that are holding the two opposite panels of formwork together.
- Adjusting the wall-filling method by using a moving inlet or multiple inlets to prevent the concrete mixture from falling several meters.
- Creating a parametric study to determine the impact of variables such as width, height, reinforcement level, and concrete mixture on the pressure exerted on the formwork.

Bibliography

[1] M. Geiker and S. Jacobsen. 10 - Self-compacting concrete (SCC). pages 229–256, 2019. https://doi.org/10.1016/B978-0-08-102616-8.00010-1.

[2] Self-Compacting Concrete. The european guidelines for self-compacting concrete. *BIBM, et al*, 22:563, 2005.

[3] H. Okamura, K. Ozawa, and M. Ouchi. Self-compacting concrete. *Structural concrete*, 1(1):3–17, 2000.

[4] N. Roussel. A thixotropy model for fresh fluid concretes: Theory, validation and applications. *Cement and Concrete Research*, 36(10):1797–1806, 2006. https://doi.org/10.1016/j.cemconres.2006.05.025.

[5] H.A. Barnes. Thixotropy—a review. *Journal of Non-Newtonian Fluid Mechanics*, 70(1): 1–33, 1997. https://doi.org/10.1016/S0377-0257(97)00004-9.

[6] Y. Asghari, E. Mohammadyan-Yasouj, and S.R. Koloor. Utilization of metakaolin on the properties of self-consolidating concrete: A review. *Construction and Building Materials*, 389:131605, 2023. https://doi.org/10.1016/j.conbuildmat.2023.131605.

[7] E.M. Aydin, B. Kara, Z.B. Bundur, N. Ozyurt, O. Bebek, and M.A. Gulgun. A comparative evaluation of sepiolite and nano-montmorillonite on the rheology of cementitious materials for 3D printing. *Construction and Building Materials*, 350:128935, 2022. https://doi.org/10.1016/j.conbuildmat.2022.128935.

[8] M. Alimohammad M. Langaroudi and Y. Mohammadi. Effect of nano-clay on workability, mechanical, and durability properties of self-consolidating concrete containing mineral admixtures. *Construction and Building Materials*, 191:619–634, 2018. https://doi.org/10.1016/j.conbuildmat.2018.10.044.

[9] Y. Li, J. Mu, Z. Wang, Y. Liu, and H. Du. Numerical simulation on slump test of fresh concrete based on lattice Boltzmann method. *Cement and Concrete Composites*, 122: 104136, 2021. https://doi.org/10.1016/j.cemconcomp.2021.104136.

[10] ASTM ASTM et al. Standard specification for flow table for use in tests of hydraulic cement. *ASTM West Conshohocken*, 1, 2014.

[11] J. Němeček, P. Trávníček, V. Zacharda, V. Pommer, and J. Němeček. Correlation of viscosimetry and practical tests of fresh cement paste consistency. *AIP Conference Proceedings*, 2322(1):020038, 02 2021. https://doi.org/10.1063/5.0042721.

[12] N. Al-Bayati. Self compacting concrete with tests. 03 2017.

[13] L. Zhou, Z. Zhang, CH. Liu, and G. Shi. Experimental and numerical investigation of axially loaded L-shaped box-T section columns. *Engineering Structures*, 291:116412, 2023. https://doi.org/10.1016/j.engstruct.2023.116412.

[14] M.S. Abo Dhaheer, S. Kulasegaram, and B.L. Karihaloo. Simulation of self-compacting concrete flow in the J-Ring test using smoothed particle hydrodynamics (SPH). *Cement and Concrete Research*, 89:27–34, 2016. https://doi.org/10.1016/j.cemconres.2016.07.016.

[15] E. Koehler, D. Fowler, A. Jeknavorian, J. Schemmel, and S. Dean. Comparison of Workability Test Methods for Self-Consolidating Concrete. *Journal of Astm International*, 7, 02 2010.

[16] J. Mu, Y. Li, C. Jin, Y. Liu, H. Li, and J. Liu. Simulation of V-tunnel test for fresh concrete on the basis of lattice Boltzmann method. *Cement and Concrete Composites*, 133:104728, 2022. https://doi.org/10.1016/j.cemconcomp.2022.104728.

[17] T.Y. Shin and J.H. Kim. First step in modeling the flow table test to characterize the rheology of normally vibrated concrete. *Cement and Concrete Research*, 152:106678, 2022. https://doi.org/10.1016/j.cemconres.2021.106678.

[18] A. Laskar. Correlating Slump, Slump Flow, Vebe and Flow Tests to Rheological Parameters of High-Performance Concrete. *Materials Research-ibero-american Journal of Materials - MATER RES-IBERO-AM J MATER*, 12, 03 2009.

[19] W.-C. Jau and C.-T. Yang. Development of a modified concrete rheometer to measure the rheological behavior of conventional and self-consolidating concretes. *Cement and Concrete Composites*, 32(6):450–460, 2010. https://doi.org/10.1016/j.cemconcomp.2010.01.001.

[20] R. Mandal, S.K. Panda, and S. Nayak. Rheology of concrete: Critical review, recent advancements, and future prospectives. *Construction and Building Materials*, 392:132007, 2023. https://doi.org/10.1016/j.conbuildmat.2023.132007.

[21] J.K. Lee, J. Ko, and Y.S. Kim. Rheology of Fly Ash Mixed Tailings Slurries and Applicability of Prediction Models. *Minerals*, 7:165, 09 2017.

[22] M. Jolin, J.-D. Lemay, N. Ginouse, B. Bissonnette, and É. Blouin-Dallaire. The effect of spraying on fiber content and shotcrete properties. 10 2015.

[23] M.S. Ramsey. Chapter Six - Rheology, Viscosity, and Fluid Types. In M.S. Ramsey, editor, *Practical Wellbore Hydraulics and Hole Cleaning*, Gulf Drilling Guides, pages 217–237. Gulf Professional Publishing, 2019. https://doi.org/10.1016/B978-0-12-817088-5.00006-X.

[24] N. Roussel, M.R. Geiker, F. Dufour, L.N. Thrane, and P. Szabo. Computational modeling of concrete flow: General overview. *Cement and Concrete Research*, 37(9):1298–1307, 2007. https://doi.org/10.1016/j.cemconres.2007.06.007.

[25] B. Zhaidarbek, A. Tleubek, G. Berdibek, and Y. Wang. Analytical predictions of concrete pumping: Extending the Khatib–Khayat model to Herschel–Bulkley and modified Bingham fluids. *Cement and Concrete Research*, 163:107035, 2023. https://doi.org/10.1016/j.cemconres.2022.107035.

[26] J.M. Khatib. Metakaolin concrete at a low water to binder ratio. *Construction and Building Materials*, 22(8):1691–1700, 2008. https://doi.org/10.1016/j.conbuildmat.2007.06.003.

[27] M. Harikaran, S. Gokulakannan, A. Loganathan, R.D. Chandiran, M. Ajith, and V. Dhanasekar. Metakaolin cement concrete evaluation using industrial by-products as fine aggregate. *Materials Today: Proceedings*, 2023. https://doi.org/10.1016/j.matpr.2023.04.586.

[28] D.A. Ammosov, N.V. Malysheva, and L.S. Zamorshchikova. Generalized multiscale finite element method for language competition modeling I: offline approach. *Journal of Computational and Applied Mathematics*, 442:115731, 2024. https://doi.org/10.1016/j.cam.2023.115731.

[29] Y. Efendiev and T.Y. Hou. *Multiscale finite element methods: theory and applications*, volume 4. Springer Science and Business Media, 2009.

[30] K. Ho-Le. Finite element mesh generation methods: a review and classification. *Computer-Aided Design*, 20(1):27–38, 1988. https://doi.org/10.1016/0010-4485(88)90138-8.

[31] Y.F. Gorgulu, M. Özgür, and R. Köse. CFD Analysis of a NACA 0009 Aerofoil at a Low Reynolds Number. *Journal of Polytechnic*, 03 2021.

[32] ANSYS Fluent et al. Ansys fluent theory guide. *Ansys Inc., USA*, 15317:724–746, 2011.

[33] G. Tryggvason. Chapter 6 - Computational Fluid Dynamics. In P.K. Kundu, I.M. Cohen, and D.R. Dowling, editors, *Fluid Mechanics (Sixth Edition)*, pages 227–291. Academic Press, Boston, sixth edition edition, 2016. https://doi.org/10.1016/B978-0-12-405935-1.00006-X.

[34] J. Haider. *Numerical Modelling of Evaporation and Condensation Phenomena*. PhD thesis, 08 2013.

[35] F. Garoosi and K. Hooman. Numerical simulation of multiphase flows using an enhanced Volume-of-Fluid (VOF) method. *International Journal of Mechanical Sciences*, 215: 106956, 2022. https://doi.org/10.1016/j.ijmecsci.2021.106956.

[36] H. Enwald, E. Peirano, and A.-E. Almstedt. Eulerian two-phase flow theory applied to fluidization. *International Journal of Multiphase Flow*, 22:21–66, 1996. https://doi.org/10.1016/S0301-9322(96)90004-X.

[37] D. Adalsteinsson and J.A. Sethian. A Fast Level Set Method for Propagating Interfaces. *Journal of Computational Physics*, 118(2):269–277, 1995. https://doi.org/10.1006/jcph.1995.1098.

[38] X. Nan, X. Liu, L. Chen, Q. Yan, and J. Li. Study of the bridge damage during flooding based on a coupled VOF-FSI method. *Journal of Engineering Research*, 11(3):51–61, 2023. https://doi.org/10.1016/j.jer.2023.100081.

[39] L. Peng, W. Xu, J. Wang, Y. Liu, W. Qian, S. Wang, T. Xie, and J. Shan. Optimization of bronchoalveolar lavage fluid volume for untargeted lipidomic method and application in influenza a virus infection. *Journal of Pharmaceutical and Biomedical Analysis*, 236: 115677, 2023. https://doi.org/10.1016/j.jpba.2023.115677.

[40] D. Lopes, R. Agujetas, H. Puga, J. Teixeira, R. Lima, J.P. Alejo, and C. Ferrera. Analysis of finite element and finite volume methods for fluid-structure interaction simulation of blood flow in a real stenosed artery. *International Journal of Mechanical Sciences*, 207: 106650, 2021. https://doi.org/10.1016/j.ijmecsci.2021.106650.

[41] N. Roussel, J. Spangenberg, J. Wallevik, and R. Wolfs. Numerical simulations of concrete processing: From standard formative casting to additive manufacturing. *Cement and Concrete Research*, 135:106075, 2020. https://doi.org/10.1016/j.cemconres.2020.106075.

[42] A. Gram. Numerical Modelling of Self-Compacting Concrete Flow - Discrete and Continuous Approach. *Bulletin*, 2009.

[43] R. Deeb, S. Kulasegaram, and B.L. Karihaloo. 3D modelling of the flow of self-compacting concrete with or without steel fibres. Part II: L-box test and the assessment of fibre reorientation during the flow. *Computational Particle Mechanics*, 1:391–408, 2014.

[44] S. Kulasegaram and B.L. Karihaloo. Assessing the flow characteristics of self-compacting concrete via numerical simulations of flow tests. pages 173–182, 01 2018.

[45] K. Vasilic, A. Gram, and J.E. Wallevik. Numerical simulation of fresh concrete flow: insight and challenges. *Publisher*, 2019. https://doi.org/10.21809/rilemtechlett.2019.92.

[46] S. Tichko, J. Maele, N. Vanmassenhove, G. De Schutter, J. Vierendeels, R. Verhoeven, and P. Troch. Numerical modelling of the filling of formworks with self-compacting concrete. *WIT Transactions on Engineering Sciences*, 69, 08 2010.

[47] S. Shanmughan and R.K. M. Modelling of Formwork Pressure Using Self-Compacting Concrete by Numerical Methods for Attaining Environmental Sustainability. *Key Engineering Materials*, 692:119–128, 05 2016.

[48] S. Tichko. *Hydrodynamic modelling of the flow of self-compacting concrete in formworks*. PhD thesis, Ghent University, 2016.

[49] J.-C. Labuschagne. Formwork pressures by self-compacting concrete: a practical perspective. *Thesis (MEng)–Stellenbosch University*, 2018.

[50] T. Richter. *Fluid-structure Interactions: Models, Analysis and Finite Elements*. Lecture Notes in Computational Science and Engineering. Springer International Publishing, 2017.

[51] ICEM Ansys. CFD User's Manual. *Ansys Inc*, 2016.

[52] A. Acharya, S. De Chowdhury, F.P. Paloth, and R. Datta. Numerical investigation of bottom slamming using one and two way coupled methods of S175 hull. *Applied Ocean Research*, 139:103684, 2023. https://doi.org/10.1016/j.apor.2023.103684.

[53] K. Wijesooriya, D. Mohotti, A. Amin, and K. Chauhan. Comparison between an uncoupled one-way and two-way fluid structure interaction simulation on a super-tall slender structure. *Engineering Structures*, 229:111636, 2021. https://doi.org/10.1016/j.engstruct.2020.111636.

[54] L. Feng, H. Gao, and X. Luo. Whole-heart modelling with valves in a fluid–structure interaction framework. *Computer Methods in Applied Mechanics and Engineering*, 420: 116724, 2024. https://doi.org/10.1016/j.cma.2023.116724.

[55] T. Nakata and H. Liu. A fluid–structure interaction model of insect flight with flexible wings. *Journal of Computational Physics*, 231(4):1822–1847, 2012. https://doi.org/10.1016/j.jcp.2011.11.005.

[56] H. Truong, T. Engels, D. Kolomenskiy, and K. Schneider. A mass-spring fluid-structure interaction solver: Application to flexible revolving wings. *Computers and Fluids*, 200: 104426, 2020. https://doi.org/10.1016/j.compfluid.2020.104426.

[57] M. Price, A. Lee, O. Soto, O. Yin, and K. Chong. FSI simulations for explosions very near reinforced concrete structures. 06 2011.

[58] T. Kraisee, P. Hankhuntod, and N. Ketchat. Analysis of Concrete Load in Very Long Column Formwork by Using Finite Element. *International Journal of Smart Grid and Clean Energy*, 12(4):100–110, 2023.

[59] ANSYS, Inc. *ANSYS Mechanical APDL Element Reference*. ANSYS, Inc., Canonsburg, PA, USA, 2021.

[60] V. Zacharda. *Effect of concrete composition and movement of formwork on horizontal pressures on the formwork*. PhD thesis, Czech Technical University in Prague, 2022.